Chemistry Africa (2024) 7:1707–1727
https://doi.org/10.1007/s42250-023-00866-2

REVIEW

Overlooked Adsorptive Route and Challenges in Arsenic Decontamination Using Iron Oxide Nanomaterials

Uttam Kumar Sahu[1,2] · Sandip Mandal[2,3] · Shengyan Pu[2]

Received: 5 May 2023 / Accepted: 18 December 2023 / Published online: 26 January 2024

Abstract
Heavy metal such as arsenic in water has gained major global attention because of their carcinogenicity to a living being in the environment. By different routes, arsenic enters the water environment and decreases the water quality even at a very lower concentration (parts of billion (ppb)). Several approaches have been studied for arsenic abatement, but the adsorption process is efficient and economical to decontaminate water from arsenic. Iron oxide nanoparticles (IONPs) can act as low-cost adsorbents because of their magnetic properties, abundance, biocompatibility, and high selectivity towards arsenic. Further to increase the adsorption capacity of IONPs, a sustainable approach has been taken, and decorated with several materials such as activated carbon, biochar, chitosan, cellulose, and mining waste materials (which are environmentally friendly, low cost, number of functional groups, high reactivity, thermal stability, chemical stability and easily available everywhere). This review has outlined the overlooked adsorptive routes for arsenic removal with importance on arsenic sources, pollution, and removal strategies. A detailed influence parameter for arsenic removal by iron oxide and iron oxide-based composite and the interaction of arsenic species with the various functional groups of adsorbents were studied.

Keywords Iron oxide nanoparticles · Composite · Arsenic · Adsorption · Removal

1 Introduction

1.1 Water Pollution

Without water, the sustainability of life cannot be imagined. The level of both surface and groundwater is decreasing day by day and only 3% of usable water is present on the earth's surface apart from groundwater [1]. This warns that very less amount of freshwater is available on the earth's surface to fill up the necessity of living beings. A recent report from the World Health Organization (WHO) shows that about one billion people don't find usable drinking water and four billion people will rigorously be affected by the shortage of drinking water by 2050 [2, 3]. Despite that, every second thousands of tons of toxic materials are coming to the water sources (pond, rivers, well, etc.) and creates problems for living beings [4, 5]. This water pollution or water quality degradation is mainly due to rapid population growth, urbanization, and industrial growth [6]. Every day tons of waste materials from different sources are coming to the natural water sources and pollute water severely as they contain pharmaceutical waste, dyes, toxic heavy metals, pesticides, organic solvents, and other pollutants [7–12].

Heavy metals are high-density elements and one of the prime toxic pollutants in water. These elements are coming to the water environments through different natural and anthropogenic activities which create problems in public health and ecology [13, 14]. However, the trace elements like iron (Fe), selenium (Se), chromium (Cr), cobalt (Co), magnesium (Mg), copper (Cu), nickel (Ni), zinc (Zn), manganese(Mn) and molybdenum(Mo) are the essential heavy metals (within their tolerance value) for the physiological and biochemical functioning of the living organisms [14, 15]. But heavy metals like lead (Pb) [16], cadmium (Cd) [17], mercury (Hg) [18], chromium (Cr) [19], and arsenic

✉ Uttam Kumar Sahu
sahuuttam02@gmail.com; uttamsahu@giet.edu

[1] Department of Chemistry, GIET University, Gunupur 765022, Odisha, India

[2] State Key Laboratory of Geohazard Prevention and Geoenvironment Protection, Chengdu University of Technology, Chengdu 610059, Sichuan, China

[3] School of Earth Sciences and Environmental Engineering, Gwangju Institute of Science and Technology (GIST), Gwangju 61005, Republic of Korea

(As) [20] are very toxic and can damage the organ even at minute concentration. Also, these elements are categorized as 'probable' or 'known' carcinogens by different environmental agencies. Figure 1 shows the problems that occur due to these heavy metals. Arsenic has secured the first position in the toxic elements list and is very toxic as compared to others, so details of arsenic are studied in this review.

1.2 Arsenic

Arsenic is a toxic metalloid with a density of 5.75 g/cm^3, an atomic weight of 74.92 amu, a boiling point of 613 °C, and a melting point of 817 °C [21]. The main reasons for arsenic contamination in water are volcanic eruption, industrial chemical waste disposal, uses of arsenic in the coating, printing pigments, dyes, microbiological activities, rapid practices of arsenic fertilizers, and burning of fossil fuels [22, 23]. Around the world, several countries (India, Pakistan, Bangladesh, China, Taiwan, Vietnam, Japan, United States, Canada, New Zealand, Argentina, Poland, Mexico, and Hungary) have drinking water problems as the arsenic concentration is very much high (0.1–73 mg/L) in both ground and surface water [24, 25]. According to the World Health Organization (WHO) guidelines, the maximum contaminant limit (MCL) of arsenic in drinking water is 0.01 mg/L. Previously the arsenic MPL was 0.05 mg/L, but in January 2006, the United States environmental protection agency disclose new guidelines and reduce the standard of concentration from 0.05 to 0.01 mg/L [26]. Arsenic is present in both organic (monomethyl arsenic acid (MMA), dimethylarsinic acid (DMA), arsine derivatives, etc.) and inorganic (arsenous and arsenic acid) forms in water [22]. Among these, organic arsenic is less toxic as it is soluble and less mobile as compared to inorganic arsenic. Again the inorganic arsenic is found in different oxidation states like + 3, + 5, 0, and -3 [27], but two major oxidation states of inorganic arsenic are As(III) (arsenite) and As(V) (arsenate) [28]. These arsenic species in the aquatic environment are extremely pH-dependent. Figure 2 shows the different speciation of As(III) and As(V) concerning pH and redox potential respectively [29]. Arsenite (As(III)) is the predominant species in anaerobic reducing environmental conditions and is present as hard arsenious acid (H_3AsO_3, $H_2AsO_3^-$ and $HAsO_3^{2-}$) while arsenate (As(V)) is the main species in oxidizing aerobic environmental conditions and occurs in soft arsenic acid (H_3AsO_4, $H_2AsO_4^-$, $HAsO_4^{2-}$ and AsO_4^{3-}) [27, 30]. As(III) is comparatively 20 times more toxic than As(V) as it reacts faster rate to the biological system [31]. As(III) is directly attached to the body protein through sulfhydryl groups and rapture the enzyme activities of the body, while As(V) can replace the phosphate groups in the mitochondria, which disturbs the oxidative phosphorylation cycles and affects the energy bond formation of adenosine triphosphate [22, 32, 33]. Hence, both oxidation states are toxic in different environmental conditions.

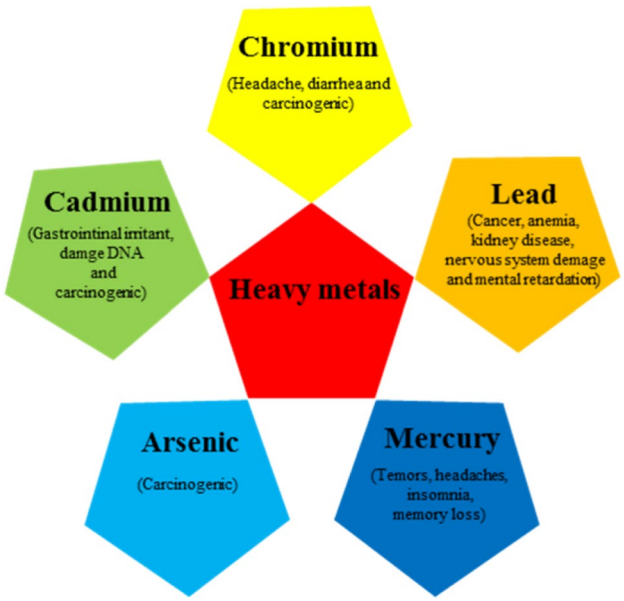

Fig. 1 Toxicity of heavy metals

1.3 Sources of Arsenic

Both natural processes and man-made activities are liable for the existence of arsenic in a usable water environment. Naturally, arsenic is mainly present in 245 types of minerals including arsenopyrite (FeAsS), realgar (As_4S_4), orpiment (As_2S_3), and enargite (Cu_3AsS_4) which are the most common mineral found in nature [34]. The report indicates that erosion and leaching of these arsenic-containing minerals results in the release of arsenic into aquatic environments [35]. Another important thing is that about 0.5–2.4 µg/g and 3–10 µg/g of arsenic also present in rocks and sediments and the leaching of these materials brings arsenic to the water system [36]. Some other natural activities like volcanic erosion, geothermal water, soil media, seasonal flooding, and sedimentation are key processes for the presence of arsenic in water systems [37–43]. On the other side of view, the main sources of arsenic in water are the day-to-day activities which are done by human beings knowingly or unknowingly. Arsenic is rummage-sale used in the production of semiconductors, lasers, transistors, and solar cells, processing of ceramics, glass, paints, pigments, soaps and dyes, catalysts, metal adhesives, ammunition, and pyrotechnics [44, 45]. Hence, the waste coming from these industries brings arsenic to the water environment. Again arsenic compounds are also applied in the production of insecticides and pesticides, which transfer the arsenic to both vegetation and water system and ultimately pollute the environment. Lastly, wood

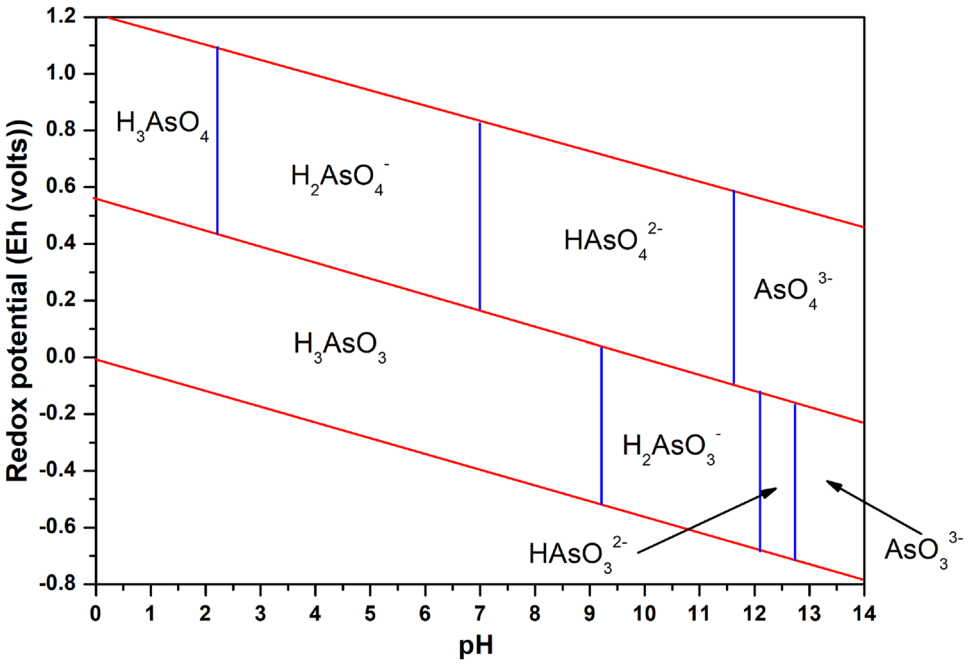

Fig. 2 Arsenic speciation at different pH according to redox potential (Eh) [29]

preservation and burning of mining have brought arsenic to 60% of the total anthropogenic activities [36].

1.4 Arsenic Toxicity

Arsenic in usable water is the major source of contact with living beings and excess concentration of arsenic in drinking water is a major environmental concern, which can cause serious carcinogenic effects to mankind [46]. Among, the top twenty hazardous elements, arsenic compounds occupy the number one position in this list as recognized by the Agency for toxic substances and disease registry (ATSDR), International Agency for Research on Cancer (IARC), and World Health Organization (WHO) [47, 48]. Arsenic exposure can occur through various routes, including ingestion, inhalation, and dermal contact. When it comes to skin exposure, arsenic can be absorbed through the skin and its ability to enter the bloodstream, could effects the vascular system, central nervous system, hematopoietic system, and cancer in the liver, skin, renal, bladder, lungs, and kidneys [22, 49]. Studies have indicated that chronic exposure to arsenic is associated with an increased risk of developing various types of cancers, such as lung, bladder, and liver cancer. Dermal exposure to arsenic can lead to skin-related health problems such as: (a) Skin Irritation: Arsenic can cause skin irritation, redness, and inflammation upon direct contact, (b) hyperpigmentation: Chronic exposure to arsenic can lead to hyperpigmentation, where patches of skin become darker in color. This is particularly evident in areas that are frequently exposed to arsenic-containing substances. (c) Keratosis: Arsenic exposure can result in the development of skin lesions known as arsenical keratoses. These are rough, scaly patches that may appear on the palms, soles, and other parts of the body and (d) Skin Cancer. Excess concentration of arsenic also enhances the glutathione peroxidase and mitochondrial superoxide dismutase (MSOD) actions in the lungs and liver [30]. Other problems like anorexia, colitis, gastritis, vomiting, diarrhoea, hair loss, weight loss, muscle cramps, hallucination, and abdominal pain happen due to acute poisoning [22]. Similarly, arsenic shows its toxic effects towards the plant species which results in changes of physiological, morphological, and metabolic properties likes decreases in chlorophyll content, short root length, membrane disruption, low photosynthetic and transpiration rate, lower relative water content of leaf, minimize the stomatal conductance, alter the sugar metabolism and production of toxic hydrogen peroxide (H_2O_2) and superoxide ions ($O_2^{\cdot-}$) in cell tissues of the plant [50, 51]. Due to arsenic poisoning, aquatic species like fish is highly affected and higher exposure of arsenic leads to alter the antioxidant enzyme activity, increase the oxidative stress, and modulation of antioxidant system of liver respectively [52].

1.5 Arsenic Removal Technologies

Several remediation technologies (membrane filtration, precipitation, ion exchange, and adsorption as shown in Fig. 3) have been applied to reduce the arsenic concentration in industrial and agricultural wastewater [53]. A detailed analysis of these arsenic removal technologies is presented in Table 1. The membrane filtration process for arsenic removal is an advanced technique and the output results are also very

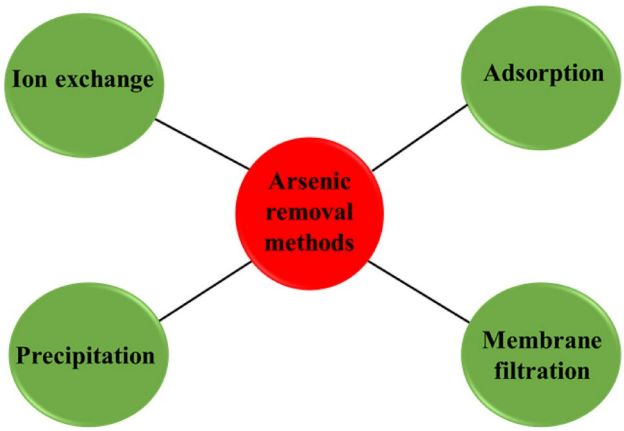

Fig. 3 Different arsenic removal methods

good [54, 55]. Different types of membranes are used concerning selective pollutants and are also used without any chemicals. But the main disadvantages of these techniques are high maintenance cost, high-pressure wastewater rejection, problems with regeneration and repeated use, and difficulty to remove As(III) [56]. Precipitation/flocculation is a different type of process for arsenic removal where aluminium, calcium, and iron salts are used to precipitate arsenic as aluminium arsenate, calcium arsenate, and ferric arsenate [53]. This process applies to the high concentration of arsenic (above 0.1 mg/L) and is difficult to remove low-concentration arsenic. Hence secondary treatments require for arsenic removal in every one cycle of experiment in the precipitation/flocculation process. Again difficult to remove As(III), hence oxidants are required to convert As(III) to As(V) [57]. One more physicochemical process is the ion-exchange process, arsenic is removed with some other ions in water [58]. Here, a column with different types of ion-exchange resin (cation-exchange resins, anion-exchange resin, and chelating resin) are inserted and arsenic water is passed through it, and an exchange of ions takes place. But this method highly depends on arsenic concentration, pH, other anions and types of resin used [24]. Hence, most of these technologies are costly, has high water discharge with secondary sludge production, and can remove the high initial concentration of arsenic but fail for lower concentrations. Thus these processes are unable for real practical application in rural areas where it is not possible for high operational setup. In the adsorption process, the adhesion of arsenic takes place on the adsorbent surface. This process can be used for practical applications of arsenic removal as the process is effective in terms of low maintenance, highly efficient, and possible to recover arsenic from the adsorbent surface [24, 59]. Here, the adsorbent can be reused many times with successful regeneration [60]. In the adsorption process, the selectivity of adsorbent plays a crucial role and these days' nanomaterials have gained visible attraction in adsorption studies [61]. The high surface area of nanomaterial provides strength and active sites which will increase the removal rate. The nanoparticles commonly used as an adsorbent for arsenic removal are aluminium [62], cerium [63], magnesium [64], manganese [65], titanium [66], zinc [67], and zirconium [68]. Compared to other environmentally friendly iron oxide has more attraction towards arsenic with magnetic separation properties offering it a suitable adsorbent. But single iron oxide nanoparticles are agglomerated which decreases the efficiency for removal studies. Therefore, modifications are done with zeolite [69], mixed oxide [9], polymeric membrane [70], activated carbon [71], graphene oxide [72], etc. to increase the performance of iron oxides and a higher percentage of As(III) and As(V) are removed.

2 Iron Oxide-Based Adsorbents for Arsenic Removal

Iron oxide nanoparticles are frequently implemented in wastewater remediation. Iron oxide and iron oxide-based adsorbents are used for arsenic removal for their unique properties. Many iron oxide nanoparticle supporting

Table 1 Advantages and disadvantages of different arsenic removal techniques

Removal methods	Advantages	Disadvantages	References
Membrane filtration	Separated by size, no phase change, advanced technique, low energy required, good output	Membrane fouling effect, expensive, high flow rates, high maintenance cost	[54, 55]
Precipitation	Simple, good sludge setting, bacterial inactivation capacity, efficient for insoluble contaminants	Generate a large volume of sludge, no reusable chemical produced, pH-dependent, require additional treatment and low removal for arsenic	[53]
Ion exchange	Simple, easy control and maintenance, rapid, efficient technology	Selective, high cost, large volume requires, precipitation causes blocking of the reactor, pH-sensitive, and resin elimination	[24]
Adsorption	Use on a laboratory scale, low cost, high efficiency, used several times	Nano-sized adsorbents require host materials, regeneration could result in secondary pollution	[24, 59]

materials are used in several studies but some of them are very costly, toxic in nature, not biodegradable, technically not feasible, have complex synthesis processes, and are unstable at normal room temperature [39, 73]. In this review, iron oxide decorated on the surface of low-cost, easily available, and environmentally friendly materials is discussed thoroughly. The materials sources, synthesis, and iron oxide decoration have been discussed. The properties of synthesizing materials are explained with suitable characterization techniques. The optimum arsenic removal conditions obtained from every study have been analyzed. The adsorption capacity obtained from the different materials has been compared with each other. The adsorption mechanism of arsenic to the adsorbent surface has been explained respectively.

2.1 Iron Oxide Nanoparticles for Arsenic Removal

Iron oxide nanoparticles (Fe_3O_4, Fe_2O_3, FeOOH, nZVIO) have a greater ability towards arsenic. Therefore, studies have been done using these iron oxide nanoparticles for wastewater treatment due to arsenic contaminations. A detailed analysis of iron oxide nanoparticles synthesis process with surface area and different conditions for arsenic removal are presented in Table 2. Raul et al. synthesized a nanoflower iron oxide hydroxide for As(III) removal [74]. Here, the Field emission scanning electron microscopy (FESEM) image confirmed the formation of nanoflower, and after As(III) adsorption changes were obtained respectively, as presented in Fig. 4. They obtained the optimum condition of adsorbent dose 1.0 g/L, contact time 300 min, pH 7.28, stirring speed 180 rpm, and temperature 25 °C for maximum As(III) removal with the uptake capacity was 475 µg/L respectively. Desorption of arsenic from exhausted IOH nanoparticles was achieved through regeneration using dilute solutions of HCl (0.5 M) and NaOH (0.2 M and 0.55 M). A desorption efficiency of 75% was observed when NaOH was utilized, whereas HCl as an eluent recorded a desorption efficiency of 54%. Again, a combination of magnetite (55.8 wt%) and maghemite (44.2 wt%) nanoparticles was synthesized by the electrical wire explosion process for the removal of arsenic [75]. Here, 20 cm long 0.3 mmø iron wires were exploded with a capacitance of 3.5 µF and voltage of 11.4 kV respectively, after which iron oxide nanoparticles were formed. It had a high magnetic saturation value of 92.4 emu/g and a surface area of 12 m^2/g respectively. XRD studies confirmed that it had a mixture of maghemite and

Table 2 Iron oxide nanoparticles synthesis process with surface area and different conditions for arsenic removal

Adsorbent	Synthesis process	Surface area (cm^3/g)	Arsenic	Optimum conditions	Isotherm	q_{max} (mg/g)	References
Iron oxide hydroxide	Precipitation	6.577	As(III)	pH 7.28; time 180 min; initial conc. 0–1000 µg/L	Redlich–Peterson	0.475	[74]
Iron oxide nanoparticles	Electrical wire explosion	12	As(III) As(V)	pH 6; time 24 h; initial conc. 1–7 mg/L pH 6; time 24 h; initial conc. 1–7 mg/L	Langmuir Langmuir	2.9 3.1	[75]
Magnetite particles	Commercial	–	As(III) As(V)	pH 2; time 3 h; initial conc. 2 mg/L pH 2; time 3 h; initial conc. 2 mg/L	Langmuir Langmuir	3.70 3.70	[77]
Fe_3O_4 nanoparticles	Microemulsion	84.68	As(III)	pH 7.7, time 120 min; initial conc. 32.32 mg/L	Langmuir	7.18	[80]
γ- Fe_2O_3	precipitation	100	As(III)	pH 5–7.5; time 1 h; initial conc. 100 mg/L	Freundlich	45	[81]
Mixed α- Fe_2O_3 and γ- Fe_2O_3	dispersion-precipitation	121	As(III)	pH 7; time 200 min; initial conc. 0–60 mg/L	Langmuir	46.5	[82]
γ-Fe_2O_3 nano chains	Flame synthesis	151.12	As(V)	pH 7; time 45 min;	Langmuir	162	[83]
Fe_3O_4 nanoaprticles	Precipitation	–	As(III)	initial conc. 0.25–	Langmuir	–	[84]
Nano zerovalent iron	Commercial		As(V)	300 mg/L	Langmuir	–	[84]
			As(III)	pH 8; time 2 min; initial conc. 50–200 mg/L pH 8; time 2 min; initial conc. 50–200 mg/L pH 6.6–6.8; time 60 min; initial conc. 10 mg/L	–	–	[85]

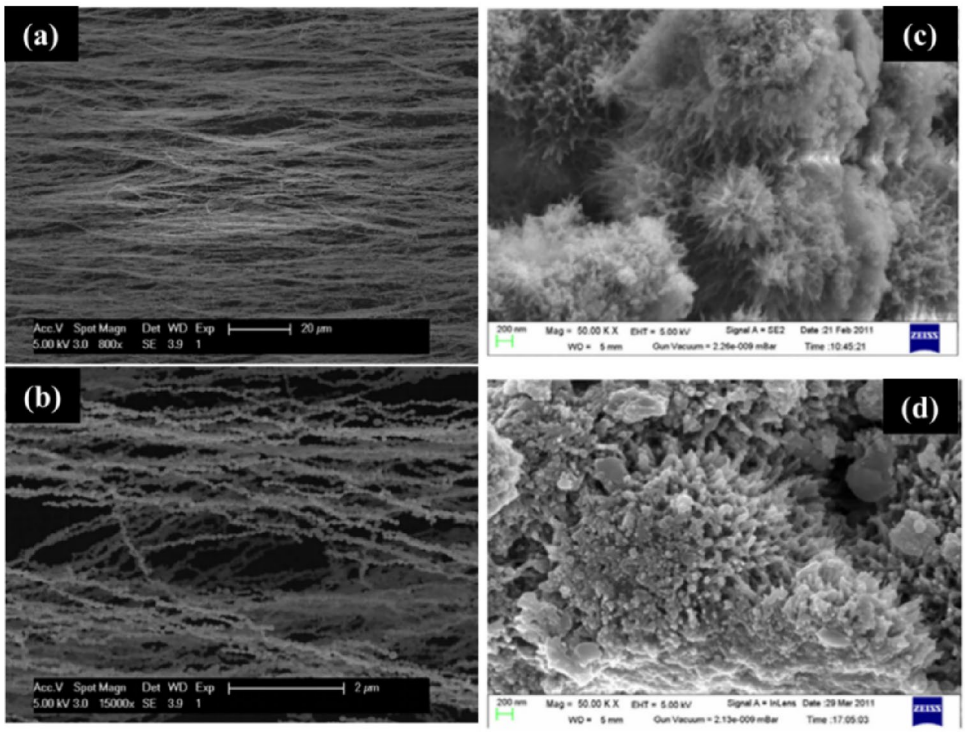

Fig. 4 SEM images of the ultra-long nano chains of iron oxides (**a**, **b**) [83] and FESEM of iron oxide hydroxide nanoparticles before (**c**) and after (**d**) adsorption of As(III) [74]

magnetite phases. The adsorption capacity was 2.9 mg/g for As(III) and 3.1 mg/g for As(V) respectively. Some researchers showed that laboratory-prepared iron oxide nanoparticles were much more efficient than commercial nanoparticles. Mayo et al. synthesized 12 nm size nanoparticles and were able to remove 98% of As(III) and As(V) respectively. The findings demonstrate a significant impact of nanoparticle size on the adsorption and desorption of arsenic, with no loss of Fe_3O_4 nanoparticles being observed. The results indicate irreversible desorption of both As(III) and As(V) from 20 nm Fe_3O_4 nanoparticles, with approximately 1% of the adsorbed As(III) and As(V) being desorbed at pH 6.1[76]. Choudhury et al. also applied commercial Fe_3O_4 nanoparticles having a size of 20 nm for As(III) and As(V) removal. Furthermore, the study found that arsenic removal from contaminated water depends on various factors, including pH, contact time, initial arsenic concentration, phosphate concentration, and adsorbent concentration. The results suggest that the adsorption of arsenic involves the formation of weak arsenic-iron oxide complexes on the surface of magnetite particles. These findings indicate the potential application of magnetite particles in the design of permeable reactive barriers for groundwater remediation, particularly for in situ remediation of groundwater contaminated with redox-active metals [77]. Here, the spontaneous nature of the adsorption process was found from the thermodynamic study with ΔG value − 35.5 kJ/mol. About 2 g/L adsorbent was enough to remove 95% of arsenic from water and the approximate adsorbent cost was 0.09$ to remove arsenic from one-liter water. They concluded that at pH 2, the maximum amount of arsenic was removed and the uptake capacity of Fe_3O_4 nanoparticles as obtained from the Langmuir isotherm model in synthetic and groundwater were 3.7 mg/g and 62.66 µg/g for As(III) and As(V) respectively. They had done another study also where they used mixed maghemite and magnetite nanoparticles and all other conditions were same except pH 6.5 [78]. The adsorption capacity was 4.75 mg/g for As(III) and 4.85 mg/g for As(V) respectively. Luther and coworkers also found good results for As(III) and As(V) by using Fe_3O_4 and Fe_2O_3 nanoparticles [79]. They had done comparison studies between both iron oxide nanoparticles and found that the adsorption capacity of Fe_3O_4 was 5680 µg/g and 4780 µg/g for As(III) and As(V). Which was lower than the adsorption capacity of Fe_2O_3 nanoparticles of 20,000 µg/g and 4904 µg/g for As(III) and As(V) respectively. In further studies, Fe_3O_4 nanoparticles were synthesized by the microemulsion process using a low-cost phosphate-free surfactant Extran and used for As(III) removal [80]. Very small size 5 nm particles were formed with a magnetic saturation value of 47 emu/g, which was high enough for rapid magnetic separation in 20 s. Here, the Box-Behnken Design model was used for As(III) removal, and 90.5% of As(III) was removed in the obtained optimum condition of adsorbent dose 0.7 g/L, initial concentration of 33.32 mg/L, and pH 7.7 respectively. In another experiment, As(V) was removed by using γ- Fe_2O_3 nanoparticles [81]. The obtained particle size was very less nearly 10 nm, hence it had superparamagnetic with a magnetic saturation value of 39.6 A m^2/kg. They observed that when the synthesis condition was Fe: As 20:1, 100% As(V)

was removed and the material had an adsorption capacity of 45 mg/g respectively. The study also noticed that as the pH increases to an alkaline environment, the efficiency of arsenate adsorption from the solution gradually decreases due to the repulsive electrostatic effect. This effect could be potentially harnessed for regenerating the adsorbent. However, the study did not present any data regarding the desorption process. Cheng et al. also prepared mixed α and γ Fe_2O_3 nanoparticles in the dispersion-precipitation method for As(III) removal [82]. In the synthesis of iron oxide nanoparticles, they used acetone for precipitation, and the final materials were calcined for 2 h at 100–500 °C (named FeMag100–FeMag500) respectively. In the FTIR studies, the methyl group vibrations (1552 cm^{-1}) were seen below 200 °C but after that, it was diminished due to the decomposition of organic meiotic at the higher temperature. It had a magnetic saturation value of 20 emu/g and shows a second-order chemisorption process. Another observation was with an increase in temperature (250 to 300 °C) the surface area was a decrease from 121 to 99 m^2/g and reached 16 m^2/g at 500 °C. Hence, the final adsorption capacity for As(III) was calculated by FeMag250, which was 46.5 mg/g from the Langmuir isotherm model, respectively. In the presence of phosphate and silicate, As(III) removal rate by these nanoparticles was decreased from 93.9% to 60.9% and 78.5%, respectively. Das et al. synthesized γ-Fe_2O_3 nano chains by a novel flame synthesis process and found very ultra-small size nanoparticles of 4 nm [83]. The SEM images at lower and higher magnifications are shown in Fig. 4. The TEM image showed very beautiful hexagonal structure nanoparticles with a surface area of 151 m^2/g. This material had a very high adsorption capacity of 162 mg/g and proceeds with the second-order kinetics model. After adsorption, it was rapidly separated from arsenic solutions because of its high magnetic saturation value of 77.1 emu/g. Recently, Martinez and team used Fe_3O_4 nanoaprticles for As(III) and As(V) removal in a different way [84]. They directly used iron precursor ($FeCl_2{\cdot}4H_2O$ and $FeCl_3{\cdot}6H_2O$) to arsenic solution and found about 91% and 96% of As(III) and As(V) removed from the waste solution. In another research, zerovalent was used for As(III) removal where the research team mainly showed the role of UVA-Vis irradiation wavelength for the removal As(III) [85]. They found that under UVA-Vis irradiation the removal capacity was increased to 94% as compare to normal analysis and dark condition analysis respectively.

2.2 Activated Carbon Modified with Iron Oxide Nanoparticles

In recent days activated carbon prepared from different waste materials or commercially available activated carbon is used for arsenic removal. Its surface is negatively charged which decreases the arsenic removal efficiency and also difficulties with its separation. Hence, iron oxide modified with activated carbon helps to solve these problems, which not only increases the removal capacity but also magnetically separated from the arsenic solution. Different iron-based activated carbon adsorbent with surface area, activated carbon source, and different conditions for arsenic removal are summarized in Table 3. Pirajan et al. used activated carbon prepared from bamboo waste and applied it for both arsenite and arsenate removal [86]. They synthesized bamboo activated carbon (BAC) from bamboo waste in the thermal process at a temperature of 950 °C, after that iron was modified on the BAC surface in the same process to get Fe-BAC. SEM studies of BAC indicated that it had a large porous structure which provides pores for Fe loading and ultimately increases the arsenic removal. The maximum adsorption took place at higher (pH nearly 11) for both arsenite and arsenate by BAC and Fe-BAC. The adsorption capacity for arsenite and arsenite was 0.20 and 0.28 mg/g by Fe-BAC as obtained by the Langmuir isotherm model. In another study, the waste biomass (pinewood sawdust; the carbon content was 43.25%) was collected from a wood factory in Beijing for activated carbon preparation [87]. In the thermal pyrolysis process, Fe_3O_4 nanoparticles were immersed on the activated carbon surface. The maximum adsorption for As(V) was seen in pH 8, contact time 6 h, and initial concentration of 40 mg/L. The adsorption capacity for As(V) was found to be 43.7 and 204.2 mg/g by the activated carbon and Fe_3O_4-loaded activated carbon, respectively. Maiti et al. used the Tamarind hull for activated carbon preparation and used for As(V) removal from synthetic and real groundwater [88]. Iron oxide was impregnated on the activated carbon surface by the thermal pyrolysis process. The maximum adsorption capacity of this adsorbent for As(V) was 1.17 mg/g. The adsorbent was used for real groundwater (As concentration 264 µg/L) and in the optimum condition of adsorbent dose 3 g/L, contact time 150 min, and pH 3–5, higher than 98% of As(V) was removed. The desorption of arsenic from As(V)-loaded IOITHC was investigated using aqueous solutions covering a pH range from 3 to 12. Subsequent adsorption tests using the regenerated adsorbent displayed an adsorption efficiency of approximately 80% compared to the fresh IOITHC adsorbent, with an initial As(V) concentration of 2.0 mg L^{-1}. Another agricultural by-product 'Apricot stone' was used for activated carbon (IAC) preparation and iron (oxy-hydro) oxides (Fe(II) and Fe(III)) was deposited on the IAC surface to prepare IAC-Fe(II) and IAC-Fe(III) [71]. Here As(V) adsorption studies were done with a variety of process parameters like initial As(V) concentration, pH, and temperature. The experiments performed 0.05–0.3 g adsorbent dose with 0.5, 4.5, and 8.5 mg/L As(V) concentration, pH 3, 5, and 7, and temperature 298, 318, and 338 K. The maximum adsorption took place at pH 3, and about 99.5% of As(V) was removed by IAC-Fe(III) adsorbent. The adsorption process was endothermic, and the adsorption capacity

Table 3 Different iron-based activated carbon adsorbent with surface area, activated carbon source, and different conditions for arsenic removal

Adsorbent	Activated carbon source	Arsenic	Optimum conditions	Surface area (cm^3/g)	Adsorption isotherm	q_{max} (mg/g)	References
Fe-BAC	bamboo waste	As(III) As(V)	pH 10.5; time 180 min; initial conc. 0.5 mg/L pH 10.5; time 180 min; initial conc. 0.5 mg/L	1357	Langmuir Langmuir	0.20 0.28	[86]
Iron oxide-impregnated carbon	Tamarind hull	As(V)	pH 3–5; time 150 min; initial conc. 2 mg/L	304.6	Langmuir	1.17	[88]
GAC-Fe	-	As(V)	pH 6; time 4-5 h; initial conc. 100 µg/L	876	Freundlich	1.430	[90]
IAC-Fe(III)	Apricot stone (agricultural byproduct)	As(V)	pH 3; time 5 h; initial conc. 4.5 mg/L	987	Freundlich and Dubinin–Radushkevich	3.009	[71]
(NZVI/AC)	Coal	As(III) As(V)	pH 6.5; time 72 h; initial conc. 0.20 mg/L pH 6.5; time 72 h; initial conc. 0.20 mg/L	64.9	Langmuir Langmuir	18.19 12.02	[91]
Iron oxide loaded on ACO	Activated charcoal	As(V)	pH 4; time 24 h; initial conc. 5 mg/L	26	Langmuir	27.78	[89]
Activated carbon modified with Fe_3O_4 nanoparticles	Cigarette soot	As(III) As(V)	pH 7); time 90 min; initial conc. 0.5 mg/L pH 3 As(V); time 90 min; initial conc. 0.5 mg/L	575.604	Langmuir Langmuir	80.99 107.96	[29]
Fe_3O_4-loaded activated carbon	Pinewood sawdust	As(V)	pH 8; time 6 h; initial conc. 40 mg/L	349	Langmuir	204.2	[87]

of IAC, IAC-Fe (II), and IAC-Fe(III) was 0.034, 2.023, and 3.009 mg/g, respectively.

Similarly, Yurum et al. used activated charcoal (AC) to prepare oxidized activated carbon (OAC), and iron oxide nanoparticles were deposited on its surface by microwave hydrothermal technique [89]. In microwave hydrothermal synthesis, three different times i.e., 3, 6, and 9 min were chosen for iron oxide nanoparticles decoration on AC and OAC surfaces. From XRD data it was found that first β-FeOOH was formed in 3 min and within 6 min α-Fe_2O_3 was formed on the AC and OAC surface and in 9 min also same results were obtained. So in microwave heating, very little time is required for magnetic iron oxide nanoparticles deposition on AC and OAC surfaces. The adsorption process was proceeding with second-order kinetics and 99.97% of As(V) was removed in just 5 min. The maximum adsorption capacity was 27.78 mg/g. In a separate study, iron oxide (Fe) was supported on granular activated carbon (GAC) using the precipitation method for As(V) removal [82]. Column studies were conducted to investigate arsenic removal by filling the column with Fe-GAC. The column had a diameter of 2 cm and a height of 30 cm, and it was filled with 32 g of the adsorbent. Different concentrations of As(V) (100, 250, and 500 µg/L) were passed through the column at flow rates of 2.5 and 5 m/h. The maximum adsorption capacity observed was 470 µg/g at 250 µg/L and a flow rate of 2.5 m/h. Furthermore, adsorption onto GAC-Fe beds is considered a preferable method for reducing arsenic (As) concentration in water compared to co-precipitation. The adsorption process offers practical advantages, including ease of operation and management, shorter treatment times, and resulting in cleaner water production with a safer As disposal potential. GAC-Fe filters exhibit higher efficiency in adsorbing As, as well as iron (Fe) and organic pollutants, in comparison to commonly used sand filters [90].

Sahu et al. used cigarette shoots, the waste product of burned cigarettes for activated carbon preparation [29]. Fe_3O_4 nanoparticles were decorated on the cigarette shoot activated carbon (CSAC) by thermal pyrolysis process and applied to reduce As(III) and As(V) from synthetic water. The results were remarkable, and the adsorbent was used for up to five cycles without any difficulties. The maximum adsorption capacities were 80.99 and 107.96 mg/g for As(III) and As(V) at pH 3 and 7 respectively. In one more work, Zhu et al. synthesized nano zero-valent iron oxide supported on an activated carbon surface (NZVI/AC) in the chemical reduction process [91]. About 8.2% of Fe loaded on needle shape carbon surface. They mainly focused on

the effects of both cations and anions on As(III) and As(V) removal and found that phosphate and silicate anions and ferrous cations sharply decreased the removal rate. The maximum adsorption capacity for As(III) and As(V) were 18.2 and 12.0 mg/g at pH 6.5. Moreover the arsenic-loaded adsorbent, NZVI/AC, was regenerated by shaking it with 0.1 M NaOH at room temperature. Within 12 h, approximately 100% of the adsorbed arsenic was successfully desorbed by the alkaline solution. In contrast, desorption using phosphate at pH 3.5 and 6.5 only achieved stripping efficiencies of 36% and 46%, respectively.

2.3 Biochar Modified with Iron Oxide Nanoparticles

Biochar is another important material that can support iron oxide for arsenic removal. Here, the adsorbent is prepared by the direct impletion of iron oxide on the biochar surface or iron precursor loaded on the biomass surface in the pyrolysis process. The iron oxide was deposited on the inner, outer, and surface pores of biochar which would rapidly adsorb arsenic from an aqueous environment. Different iron-based biochar adsorbent with surface area, biochar source, and different conditions for arsenic removal are presented in Table 4. Hence, Zhang et al. used hyacinth biomass for biochar (MW2501) preparation and used precipitation process for iron oxide decoration on its surface, later on, used for As(V) removal [92]. This magnetic biochar had an adsorption capacity of 7.41 mg/g, as obtained from the Langmuir–Freundlich model. The maximum adsorption took place at pH 5.3 and was followed by a pseudo-second-order kinetics model. Whereas the sorbent MW2501 exhibited excellent initial As(V) removal efficiency, achieving around 100% removal at an initial concentration of 5 mg/L and a solid/solution ratio of 1:200. Upon regeneration and subsequent sorption cycles, the As(V) removal remained at approximately 80%. However, in the third and fourth cycles, the efficiency declined to 50.8–65.5%. Despite this reduction, the sorbent could still be easily separated from the solution using a magnet after four cycles and provide a cost-effective option for treating most As-containing water in nature, particularly those with As concentrations below 5 mg/L. Sometimes fibrous biochar had been synthesized to increase the As(III) and As(V) adsorption capacity [93]. Here, fibrous biochar was prepared in a furnace at 800 °C for 2 h from the cotton fiber source. Then iron oxide was decorated with fibrous biochar surface in the hydrothermal process at 120 °C for 6 h and denoted as Fe-NN/BFs. As the name indicates, the SEM image (Fig. 5) confirmed the formation of a nanoneedle array of iron oxide on the fibrous biochar surface. The maximum adsorption took place at 15 and 120 min for As(V) and As(III), followed by a second-order kinetics model. The maximum adsorption capacity was 70.22 and 93.94 mg/g for As(III) and As(V) obtained from the Langmuir model. The materials were also applied for a real arsenic-contaminated water system where the initial arsenic concentration was 275 µg/L. The As(III) concentration was reduced to 5.31 µg/L in 15 min with an adsorbent dose of 2 g/L, whereas As(V) concentration was decreased to 1.22 µg/L in 30 min using 1.5 g/L of Fe-NN/BFs.

Again, bamboo waste was used for bamboo charcoal preparation and iron oxide was modified in the precipitation process [94]. This modified adsorbent showed a good surface area of 277.875 m^2/g which would help for a higher percentage of As(III) and As(V) removal. The adsorption

Table 4 Different iron-based biochar adsorbent with surface area, biochar source, and different conditions for arsenic removal

Adsorbent	Biochar source	Arsenic	Optimum conditions	Surface area (m^2/g)	Adsorption isotherm	q_{max} (mg/g)	References
Rice husk iron oxide composite biochar	Rice husk	As(III)	pH 7.5; time 12 h; initial conc. 0.05–0.2 mg/L	300	Langmuir	0.096	[96]
Wheat husk iron oxide composite biochar	Wheat husk	As(III)	pH 7.5; time 12 h; initial conc. 0.05–0.2 mg/L	339	Langmuir	0.116	[96]
Iron-loaded biochar	Waste walnut shell	As(V)	pH 7; time 10 h; initial conc. 0.1–5 mg/L	418	Langmuir	1.19	[97]
Iron-Modified Bamboo Charcoal	Bamboo	As(III) As(V)	pH 4–5; time 30 h; initial conc. 2.343 mg/L pH 9–4; time 35.5 h; initial conc. 2.343 mg/L	277	Freundlich Freundlich	7.237 19.771	[94]
Bark-based magnetic iron oxide particles	*Tamarindus Indica*	As(III)	pH 7; time 11 h; initial conc. 92–1981 µg/L	40.87	Langmuir	19.61	[98]
Magnetic gelatin-modified biochar	Chestnut shell	As(V)	pH 4; time 24 h; initial conc. 0–50 mg/L	-	Langmuir	45.8	[95]
AMP@Fe_2O_3 nanocomposite	*Aegle marmelos*	As(V)	pH 3, time 250 min, initial conc. 0.1–50 mg/L	135.29	Langmuir	69.65	[99]

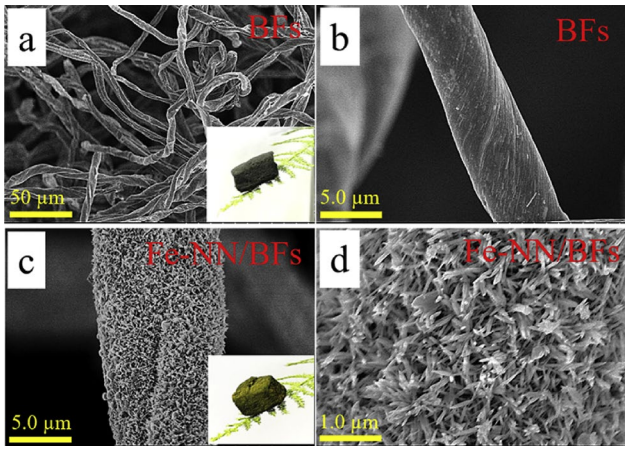

Fig. 5 SEM images of **a**, **b** BFs and **c**, **d** Fe-NN/BFs [93]

process for arsenic (As(III) and As(V)) was followed by a pseudo-second-order kinetics model with higher R^2 values than the pseudo-second-order and Elovich model kinetics model. Here, the intraparticle diffusion model showed multiple natures of the relationship and indicated a complex mechanism for As(III) and As(V). Zhou et al. prepared gelatin-modified magnetic biochar for As(V) removal [95]. Here, the chestnut shell was used for biochar formation, and gelatin a natural polymer rich in amino acids modified on the biochar surface to enhance adsorption capacity. Again magnetic iron oxide was loaded for magnetic separation of adsorbent after As(V) removal from the solution. It has a magnetic saturation value of 42 emu/g, which was high enough for magnetic separation. The kinetics studies showed that the adsorption process was chemisorption in nature and interaction took place between As(V) anions and positively charged functional groups of adsorbent through ion exchange or chelating process. The adsorption capacity was 45.8 mg/g for As(V) by gelatin-modified magnetic biochar and As–O interactions and electrostatic interactions was the main adsorption mechanism. Further two novel types of biochar were prepared from rice husks and white husks, then iron oxide was decorated on these biochar surfaces by the pyrolysis process at 600 °C for 1 h under nitrogen temperature [96]. Batch adsorption studies were performed for As(III) removal using RHIOB and WHIOB. Adsorption isotherm studies were performed at 10, 25, and 40 °C, pH 6.5–7.5 with a variation of As(III) concentration from 50 to 5000 µg/L. The output of this experimental data fitted with Langmuir, Freundlich, Temkin, Sips, Radke and Prausnitz, Redlich−Peterson, and Toth isotherms models. The different models were fitted to experimental data obtained from different temperature but adsorption capacities obtained from both cases in the Langmuir model were highly close to the experimental adsorption capacities. The As(III) adsorption capacity for RHIOB and WHIOB were 0.096 and 0.116 mg/g, respectively. In another work, the waste walnut shell was used for iron-loaded biochar (ILB) preparation in the microwave pyrolysis process where the microwave frequency was 2.45 GHz and tubular furnace power was 800 W during ILB preparation [97]. The adsorption capacity of ILB was 1.19 mg/g respectively. In another study, the bark of *Tamarindus Indica* was used to prepare biochar, and Fe_3O_4 nanoparticles were deposited on its surface by thermal pyrolysis process [98]. The materials had a surface area of 40.87 m^2/g and a magnetic saturation value of 38.62 emu/g respectively. Langmuir isotherms model was best fitted as compared to Freundlich, and Dubinin–Radushkevich isotherms models. The adsorption capacity for As(III) and As(V) calculated from the individual study was 19.61 mg/g for As(III) and 13.58 mg/g for As(V) respectively. They also showed that when both As(III) and As(V) were present in the solution, the adsorption capacity for As(III) and As(V) was 7.04 and 9.43 mg/g respectively. In another research, *Aegle marmelos* leaves (Indian bael) were used for magnetic bio-adsorbent preparation, and Fe_2O_3 nanoparticles were incorporated on its surface by pyrolysis process at 300 °C [99]. The material showed good results for As(V) removal in optimum condition of pH 3, adsorbent dose 0.1 g/L, initial concentration 0.5 mg/L and contact time 250 min. The adsorbent had an uptake capacity of 69.65 mg/g and can be used for five cycles without any problems.

2.4 Magnetic Chitosan Adsorbents

Chitosan (CS) is produced from chitin (exoskeleton of animals such as crabs, prawns, crayfish, woodlice, shrimps, lobsters, krill, and barnacles) by the deacetylation process. Hence, it is easily obtained from nature and biodegradable. It has a higher number of amino and hydroxyl groups which can act as possible adsorption sites [100]. Thus, the specific surface properties of iron oxide can be increased by chelating with CS will be more feasible for arsenic removal [101, 102]. Table 5 shows the different magnetic chitosan adsorbent with surface area and different conditions for arsenic removal. Liu et al. used chitosan and prepared magnetic chitosan nanoparticles for arsenic removal [103]. Here, the particles were 10 nm in size and about 95% of both As(III) and As(V) were removed within the time period of 15 min. The adsorption capacities observed were 60.2 and 65.5 mg/g for As(III) and As(V) respectively. This adsorbent could be used for real applications as 95% of the adsorption capacity was stable even after 10 consecutive cycles. Abdollahi et al. also used chitosan-coated Fe_3O_4 nanoparticles for As(III) removal and adsorption capacity was less about 10.5 mg/g at pH 3 by this adsorbent [104]. Chauhan and coworkers synthesized Chitosan/PVA/zerovalent iron nanofibrous (CPZ) materials in the electrospinning process to remove arsenic from water [105]. The CS fiber was formed, and a

Table 5 Different magnetic chitosan adsorbent with surface area and different conditions for arsenic removal

Adsorbent	Arsenic	Optimum Conditions	Surface area (m^2/g)	Adsorption Isotherm	q_{max} (mg/g)	References
Iron chitosan granules	As(III) As(V)	pH 7; time 4 h; initial conc. 1–10 mg/L pH 7; time 4 h; initial conc. 1–10 mg/L	96.8	Langmuir Langmuir	2.32 2.24	[109]
chitosan-coated magnetic nanoparticles	As(III)	pH 9; time 90 min; initial conc. 1–100 mg/L	–	Langmuir	10.5	
Iron chitosan flakes	As(III) As(V)	pH 7; time 4 h; initial conc. 1–10 mg/L pH 7; time 4 h; initial conc. 1–10 mg/L	1.44	Langmuir Langmuir	16.15 22.47	[109]
Magnetic chitosan biochar (MBC)	As(V)	pH 5; time 3 h; initial conc. 0.2–50 mg/L	–	Langmuir	17.876	[107]
iron-chitosan-coated sand (ICCS)	As(III) As(V)	pH 7; time 2 h; initial conc. 100–1000 mg/L pH 7; time 2 h; initial conc. 100–1000 µg/L	0.3875	Freundlich Freundlich	26 56	[108]
Magnetic chitosan nanoparticle	As(III) As(V)	pH 6.8; time 15 min; initial conc. 50 mg/L pH 6.8; time 15 min; initial conc. 50 mg/L	108.32	Langmuir Langmuir	60.2 65.5	[103]
Chitosan zerovalent iron nanoparticle	As(III) As(V)	pH 7; time 180 min; initial conc. 1–10 mg/L pH 7; time 180 min; initial conc. 1–10 mg/L	69	Langmuir Langmuir	94 119	[110]
CS functionalized iron nanocomposite	As(III)	pH 7; time 10 h; initial conc. 2–60 mg/L	111.8	Langmuir	108.6	[106]
Chitosan/PVA/zerovalent iron nanofibrous	As(III) As(V)	pH 7; time 4 h; initial conc. 0.1–10 mg/L pH 7; time 4 h; initial conc. 0.1–10 mg/L	–	Langmuir Freundlich	142.9 200	[105]

zerovalent iron oxide nanoparticle was decorated on its surface with a size of less than 100 nm. These fibrous materials showed good results for arsenic removal with high uptake capacities for As(III) (142.9 mg/g) and As(V) (200 mg/g). This CPZ adsorbent material was regenerated with 0.01 M NaOH solutions and regenerated materials removed 20% less in the fifth cycle than in fresh cycles which suggested that there was a strong interaction between adsorbent and adsorbate. Chitosan (CS) functionalized iron nanosheet was synthesized by doping method and aimed for As(III) removal [106]. Here they doped 0–0.5% CS on an iron oxide surface and CS doping was chemically confirmed by FTIR studies. Where the bends were shifted from 3340 cm^{-1} bends for $–NH_2$ decreased and 1637 cm^{-1} for –OH was moved to 1019 cm^{-1}. This confirmed that CS (0.5%) was doped on an iron oxide surface with a surface area of 118 m^2/g. Again, the As(III) removal capacity was increased with an increase in % of CS. The maximum removal was achieved at 0.5% with an uptake capacity of 108.6 mg/g.

To increase the surface area or in other words to increase the adsorption capacity of As(V), the biochar surface was modified with magnetic chitosan composite [107]. In this study, rice straw biomass was used to prepare biochar, and magnetic chitosan was modified on its surface. The authors compared two materials: chitosan-modified biochar (CB) and magnetic chitosan biochar composite (MBC) for their adsorption capabilities. MBC showed maximum adsorption compared to CB. The adsorption capacity of MBC for As(V) was 14.92 mg/g, 17.16 mg/g, and 17.876 mg/g at temperatures of 25 °C, 35 °C, and 45 °C, respectively, indicating an endothermic nature of the adsorption process with a ΔH value of 232.630 kJ/mol.

Even after After five cycles of reuse, the regenerated MCB still retained about 8.078 mg/g uptake capacity for As(V), indicating good reusability for As(V) removal. However, the decrease in adsorption capacity could be attributed to the reduction in surface area and pore volume, along with relatively weak functional groups. Another study had been done where iron-chitosan-coated sand was used for As(III) and As(V) removal [108]. Here, a comparison study had been done between chitosan-coated sand (CCS) and iron-chitosan-coated sand (ICCS). The surface area of CCS and

ICCS were 0.3978 and 0.3875 m^2/g respectively. For both As(III) and As(V), maximum removal took place at near-neutral pH. They applied this material for real water application in the Shuklaganj area of Kanpur district, UP, India where the arsenic concentration was higher than 500 µg/L. Column experiments study has been performed with ICCS and arsenic concentration reduced to less than 5 µg/L.

Gupta et al. used iron chitosan flakes (ICF) and iron chitosan granules (ICB) to remove arsenic and found an adsorption capacity of 16.15 and 2.32 mg/g for As(III) and 22.47 and 2.24 mg/g for As(V) at pH 7 by ICF and ICB adsorbent respectively [109]. Here, they performed column studies, where 112-bed volumes of As(V) and 147-bed volumes of As(III) pointed wastewater were passed through the column (filled with iron chitosan flakes) and it was found that the 500 µg/L arsenic reduces to less than 10 µg/L. Again Gupta et al. used chitosan zerovalent iron nanoparticle (CIN) for arsenic removal [110]. The adsorption capacity of CIN was 94 mg/g for As(III) and 119 mg/g for As(V), respectively. This adsorbent had higher efficiency than the previous one.

2.5 Magnetic Cellulose Nanocomposite

Currently, biopolymers like cellulose act as a promising adsorbent for arsenic removal [111, 112]. The agricultural waste product or natural fiber which is biodegradable and economical has lots of components like cellulose, lignin, protein, hemicellulose, pectin, and fatty acid. This contains several functional groups and are more suitable for surface modifications which can also be used as a source of cellulose [113–115]. Hence, a combination of these cellulose and cellulose obtained from natural materials can be combined with iron oxide and act as an efficient biocomposite with high adsorption capacity and easily recovered using an external magnet [116, 117]. Table 6 represents the different magnetic cellulose nanocomposite adsorbent with surface area, cellulose source, and different conditions for arsenic removal. Yu and their coworker synthesized cellulose-iron oxide nanoparticles to remove arsenic from aqueous solutions [118]. They used cotton as a cellulose source and Fe_2O_3 nanoparticles were dispersed on the cellulose matrix by a step precipitation process. To confirm material formation, there were characterized by XRD, TGA, XPS, FTIR, VSM, SEM, and TEM instrumental techniques. The size of Fe_2O_3 on the cellulose matrix was 61 nm and had a magnetic saturation value of 13.2 emu/g respectively. The effects of anions on arsenic removal on this adsorbent follow the order of sulfate < nitrate < phosphate. The adsorption efficiency was 23.16 and 32.11 mg/g for As(III) and As(V) respectively. In another study, Zhou et al. also synthesized cellulose-nZVI composites using medical cotton and nZVI was decorated in a reduction process [119]. The cellulose formation was confirmed with XRD peak at 22.7° (002) and 34.5° (040) respectively and nZVI formation was confirmed with 2θ of 44.7° (110) and 65.02° (200) planes of Fe^0 with JCPDS card no. 06–0696. The cellulose-nZVI composites had a saturation magnetization value of 52.7 emu/g and could be easily separated after adsorption. Maximum As(III) was removed

Table 6 Different magnetic cellulose nanocomposite adsorbent with surface area, cellulose source, and different conditions for arsenic removal

Adsorbent	Cellulose source	Arsenic	Optimum Conditions	Surface area (m^2/g)	Adsorption Isotherm	q_{max} (mg/g)	References
iron-coated honeycomb	Honeycomb	As(V)	pH 7.5; time 14 h; initial conc. 100–500 µg/L	–	Langmuir	0.961	[125]
Magnetic wheat straw	wheat straw	As(III) As(V)	pH 7; time 12 h; initial conc. 1–28 mg/L pH 3; time 12 h; initial conc. 1–28 mg/L	–	Langmuir Langmuir	3.898 8.062	[121]
Fe-JF	Jute fiber	As(III)	pH 7; time 200 min; initial conc. 1–150 mg/L	–	Langmuir	12.66	[122]
Cellulose@iron oxide nanoparticles	Cotton	As(III) As(V)	pH 7; time 4 h; initial conc. 50 mg/L pH 2; time 4 h; initial conc. 100 mg/L	113	Langmuir Langmuir	23.16 32.12	[118]
JF@Fe_2O_3 nanocomposite	Jute fiber	As(V)	pH 3; time 90 min; initial conc. 0.1–50 mg/L	95.43	Langmuir	48.06	[123]
Cellulose@nZVI composites	Medical cotton	As(III)	pH 8; time 40 min; initial conc. 10 mg/L	–	Langmuir	92.25	[119]
Tea waste to modified Fe_3O_4 nanoparticles	Tea waste	As(III) As(V)	pH 7; time 12 h; initial conc. 2 mg/L pH 7; time 12 h; initial conc. 0.2–0.8 mg/L	–	Langmuir Langmuir	188.69 153.8	[124]

at pH 8 and the adsorption capacity was 92.25 mg/g as calculated from the Langmuir model. The composite was regenerated with 0.1 M HCl solution, where the removal efficiency was 99.31%, and after use for four cycles the removal rate was 92.17% respectively. Similarly, Hokkanen et al. synthesized magnetic iron nanoparticles modified microfibrillated cellulose (FeNP/MFC) and remove As(V) from aqueous solutions [120]. 100% of As(V) was removed at pH 2 with a contact time of 75 min. The maximum adsorption capacity was 2.460 mmol/g, respectively.

Tian and their coworker synthesized magnetic wheat straw (MWS) by incorporating different Fe_3O_4 nanoparticles on the wheat straw surface [121]. Here, XRD studies of WS indicated that cellulose was the main component present on the WS, so Fe_3O_4 nanoparticles were easily attached through its functional groups present on the cellulose. MSW had a magnetic saturation value of 11.87 emu/g, which was also high enough for magnetic separations. The maximum adsorption capacity was 3.898 mg/g for As(III) and 8.062 mg/g for As(V), respectively. Hao et al. synthesized jute fiber modified with iron oxyhydroxide (FeOOH) in normal precipitation for As(III) removal [122]. First, jute fibers were esterified with succinic anhydride to graft with carboxyl groups to increase the iron(III) amount on the JF surface and the maximum Fe on the JF surface was 208.2 mg/g. They performed a comparative study between JF and Fe-JF removal efficiency for As(III). Here, iron leaching was about 0.178 mg/g to the water which meets the requirements of iron in the water. The As(III) adsorption capacity was 12.66 mg/g. Again Sahu et al. also used jute fiber and decorate Fe_2O_3 nanoparticles (JF@Fe_2O_3 nanocomposite) for As(V) removal [123]. They found that iron oxide nanoparticles were dispersed on the jute fiber surface and increased the surface area from 5 to 95 m^2/g respectively. The adsorption capacity of this composite material was 48.06 mg/g at pH 3. The kinetic was followed by the pseudo-second-order model and maximum adsorption took place in 90 min. The JF@Fe_2O_3 nanocomposite was also able to remove As(V) in the presence of other competitive ions. Similarly, Lunge et al. used tea waste to modify Fe_3O_4 nanoparticles on its surface [124]. The Fe_3O_4 nanoparticles were 5–25 nm in size which would increase the surface area. The adsorption capacity was 188.69 mg/g for As(III) and 153.8 mg/g for As(V), respectively. To synthesize 1 g of MION-Tea (magnetic iron oxide nanoparticles) adsorbent, only 136 rupees are required, and the adsorbent can be used for 5 cycles without any decrease in removal rate. To remove 100 L of As(III) contaminated water by using this MION-Tea adsorbent, the cost was only 14 rupees. Hence, this can be potentially applied to arsenic water treatment. Some researchers used novel waste like honeycomb briquette cinder and Fe_2O_3 nanoparticles decorated on its surface and used for As(V) removal [125]. They found about 961.5 µg/g of As(V) was removed at pH 7.5 and time 14 h. Langmuir's model was fitted to experimental data with an R^2 value of 0.999 and R_L value of 0.118, respectively. The other negatively charged species had the following order: $PO_4^{3-} > HCO_3^- > F^- > Cl^-$ on As(V) removal.

2.6 Iron Oxide Nanoparticles Doped Mineral Oxides Composite

In recent days minerals, and adsorbents (sand, rock, and clay materials) have been applied for wastewater treatment for their low cost, easy availability, and environmentally friendly nature [126, 127]. But due to its negative surface charge, the efficiency of arsenic is very low [128, 129]. Hence, magnetic composite materials are prepared with iron oxide nanoparticles and used to remove arsenic from wastewater [130]. Table 7 gives details information of different iron oxide doped minerals nanocomposite, surface area, mineral source, and different conditions for arsenic removal. Devi and their coworker also used iron oxide-coated sand and limestone for As(III) removal from contaminated water [130]. The As(III) removal percentage was very high and 96% to 98.6% of As(III) was removed from 100 and 400 µg/L initial concentration arsenic solution. The effect of pH studies was performed in pH 4.8, 7.1, 8.5, and pH 10.4, and a near-neutral pH maximum amount of As(III) was removed. The pseudo-second-order was more accurate to the experimental data which was performed in the arsenic concentration of 200 and 500 µg/L. Column studies were completed where column height and diameter were 120 cm and 7.0 cm respectively, then iron oxide-coated sand filled and 200 µg/L arsenic were passed through it which reduced to 10 µg/L respectively. Maji and his coworker synthesized iron-oxide-coated natural rock (IOCNR) to remove arsenic from the contaminated groundwater of Lanyang Plain, North Eastern Taiwan [131]. About 75% of arsenic was removed from real water in the optimum conditions of an adsorbent dose of 15 g/L, initial concentration of 40 µg/L, pH 7, agitation speed of 180 rpm, and contact time 6 h. The arsenic concentration was reduced to less than 10 µg/L, which is below maximum arsenic accessible limit. Here, the pH of water was 7.5 as As(III) was the major species than As(V). First order kinetic model and Langmuir isotherm models were fitted to the experimental data and adsorption was spontaneous in nature as per thermodynamic data. The maximum arsenic adsorption capacity was 0.36 mg/g. They also used this iron-oxide-coated natural rock as an adsorbent for As(III) removal in column experiments and found satisfactory results [132]. Srivastava et al. synthesized modified iron-coated sand (DMICS) for As(III) elimination from contaminated water [133]. The sand was collected from river tons in Allahabad (India). Maximum As(III) was removed in the pH range of 6.5–7.5. The isotherm study

Table 7 Different iron oxide doped minerals nanocomposite, surface area, mineral source, and different conditions for arsenic removal

Adsorbent	Source	Arsenic	Optimum Conditions	Surface area (m^2/g)	Adsorption Isotherm	q_{max} (mg/g)	References
Iron oxide-coated sand and limestone	Sand and limestone	As(III)	pH 7.2; time 2 h; initial conc. 100–400 µg/L	–	Langmuir	0.075	[130]
Iron-oxide-coated natural rock	Rock	As(III)	pH 7.5; time 6 h; initial conc. 40 µg/L	15.312	Langmuir	0.36	[131]
Iron-coated sand (DMICS)	Sand	As(III)	pH 6.5–7.5; time 8 h; initial conc. 0.5–2.0 mg/L	–	Langmuir	0.29	[133]
Iron-modified light-expanded clay	Clay	As(V)	pH 6–7; time 24 h; initial conc. 1 mg/L	–	Langmuir	3.31	[134]
Iron oxide-modified clay-activated carbon	Clay	As(V)	pH 3; time 24 h; initial conc. 5–75 mg/L	433	Langmuir	5.0	[135]
Clay-supported zerovalent iron nanoparticles	Clay	As(III)	pH 2.75–9; time 30 min; initial conc. 100 mg/L	200.66	–	–	[136]

was followed by the order Langmuir > Freundlich > Temkin with the experimental data. The obtained adsorption capacity was 0.29 mg/g respectively. Same time, iron-modified light-expanded clay was used to remove As(V), and found that the material had an adsorption capacity of 3.31 mg/g at pH 6–7 [134]. Power et al. used iron oxide-modified clay-activated carbon for As(V) removal [135]. Here, Na-alginate and coconut shells were used as a source of clay and activated carbon. The prepared adsorbent had a high surface area of 433 m^2/g, which was very high compared to single iron oxide nanoparticles. The FTIR studies suggested that a higher number of hydroxyl and carboxyl groups were present on the adsorbent surface which was responsible for As(V) adsorption. About 85% of arsenic was removed at pH 3 and decreased to 42% at pH 9 at the same time with an increase in As(V) concentration from 5 to 75 mg/L the adsorption capacity increased from 2.06 to 4.9 mg/g respectively. The adsorption experiments were done at low-level concentration and As(V) concentration was decreased from 50 to 7.45 µg/L, respectively. Some research had been done where the clay surface was decorated with zerovalent iron oxide nanoparticles for As(III) removal [136]. In the synthesis process, a green way of approach had been conducted and tea liquor was used as a reducing agent and successfully prepared nZVI on the clay surface. This adsorbent had the particle size and high surface area of 59.08 nm and 200.66 m^2/g and was able to remove 99% of As(III) over a large pH range.

3 Adsorption Mechanism

Several studies verified that the adsorption of arsenic on the iron-based adsorbent surface have been carried out by inner-sphere complexion i.e. monodentate, bidentate, and tridentate ligand exchange, electrostatic attraction, and ion exchange mechanism [137–139]. Furthermore, instrumentals such as Fourier-transform infrared spectroscopy (FTIR), and X-ray photoelectron spectroscopy (XPS) are used to elucidate the attachment of arsenic species on the adsorbent surface [114, 140].

The adsorption of As(III) on the iron oxide nanoparticles' surface was due to the inner sphere mechanism [82]. In FTIR spectra after adsorption, the appeared bend at 780 cm^{-1} was for As(III)-O stretching vibrations. This indicated that surface hydroxyl was replaced by arsenic and the Fe–O-As bond was formed. Sahu et al. had also shown that As(V) is attached to CSAC/Fe_3O_4 composite surface through both ligand exchange (monodentate and bidentate) and electrostatic attraction as shown in Fig. 6 [29]. Here, they used FTIR studies to clear the adsorption mechanism. The adsorbent had Fe-OH vibration at 1080 cm^{-1}, but after adsorption, this bend was completely removed, and two new bends were seen at 792 and 807 cm^{-1} for Fe–O–As(III) and Fe–O–As(V) vibrations respectively. This suggested that –OH groups were replaced by arsenic species by the inner sphere ligand exchange mechanism. Andjelkovic et al. also proposed similar types of adsorption mechanisms for As(III) and As(V) on the surface of iron-oxide nanowires on the basics of FTIR studies [48]. The iron-oxide nanowires had a spectrum of 952 cm^{-1} for Fe-OH bending vibration. After the adsorption of As(V) and As(III), this Fe-OH bend completely disappeared and the new bend was seen at 812 cm^{-1} for As(V)-O vibrations but in the case of As(III), the 912 cm^{-1} bends were decreased. This indicated As(V) and As(III) were attached to where –OH groups on the adsorbent surface played a major role. They also said that the As(V) was attached by electrostatic attraction of Fe-OH_2^+ groups of adsorbent and $H_2AsO_4^-$ species. Similar studies were obtained by another researcher, where the adsorption

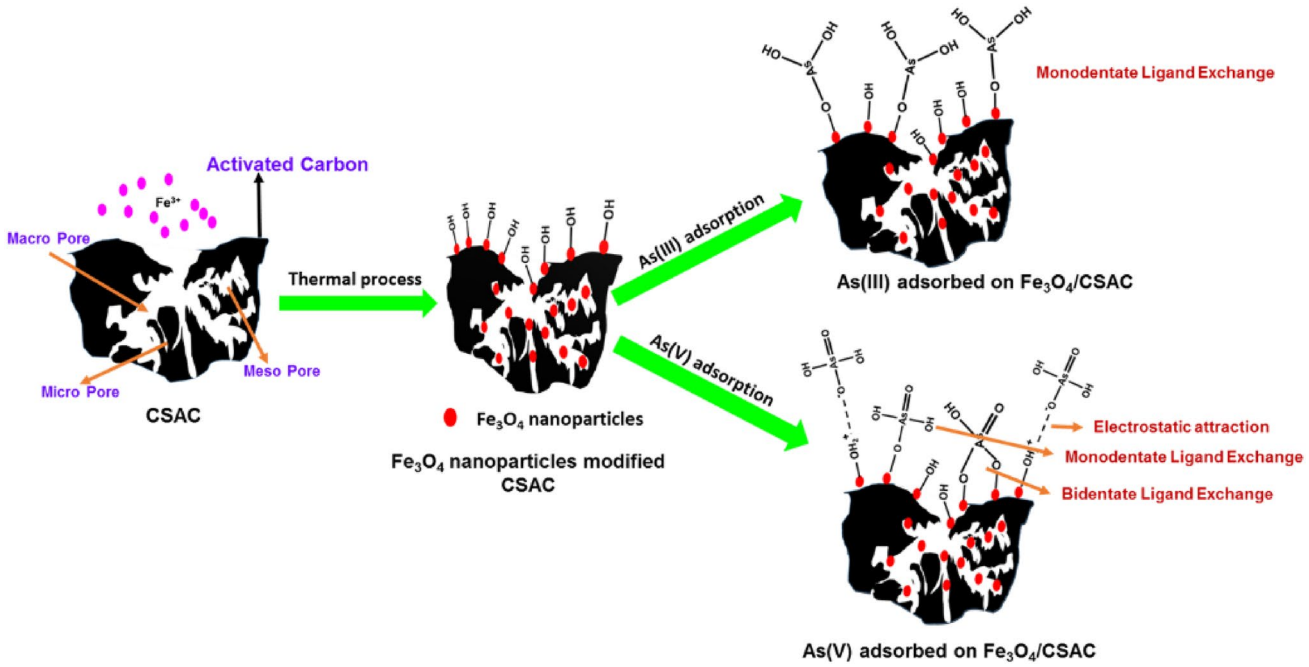

Fig. 6 Adsorption of As(III) by ligand exchange and As(V) by ligand exchange and electrostatic attraction process [29]

mechanism for As(V) to the iron oxide-loaded activated carbons was mainly due to electrostatic attraction going on between positively charged surface (Fe-OH + and Fe-OH_2^+) and negatively charged As(V) species ($H_2AsO_4^-$ and $HAsO_4^{2-}$) [71, 86–91]. They showed that below pH_{PZC} the surface had a high positive charge and maximum adsorption took place in this region and above $pH_{PZC,}$ the adsorbent had negatively charged so repulsion took place. So As(V) is attached through electrostatic attraction on the adsorbent surface.

Zhang et al. explained the As(V) adsorption mechanism on the basics of FTIR and XPS analysis. The FTIR of MW250 (magnetic biochar prepared at 250 °C) after As(V) adsorption, the bend at 3417, 3472, 3554, and 1319 cm^{-1} for surface hydroxyl groups were decreased to a negligible level, which suggested that surface hydroxyl groups attached to Fe were replaced by $H_2AsO_4^-/HAsO_4^{2-}$ groups by ligand exchange mechanism [141]. Also, the bend at 1602 cm^{-1} for C = O bend in –COO groups was decreased which suggested that a hydrogen bonding was held between –COO groups and hydroxyl groups of $H_2AsO_4^-/HAsO_4^{2-}$ [142]. XPS spectra after As(V) adsorption showed the presence of three high-resolution spectra of $As2p_{3/2}$. The peak at 1326.02 eV was for As(III) due to oxidative transformation and two other peaks at 1327.01 and 1327.67 eV were for As(V). This also suggested that As(V) was adsorbed on the MW250 adsorbent surface. The bark-based magnetic iron oxide particles for As(III) and As(V) also showed ligand exchange of hydroxyl groups [98].

The adsorption mechanism of As(III) and As(V) by Fe-NN/BFs was also examined on the basics of XPS studies. After adsorption, the binding energies of As(III) and As(V) were 44.7–5.2 eV and 45.9–46.3 eV respectively. This mainly showed that arsenic was attached to the Fe-NN/BFs surface but the mechanism was explained by O 1 s XPS patterns of Fe-NN/BFs. Before adsorption, the peak at 529.8, 531.4, and 532.5 eV represented the O lattice of MO, O in hydroxyl groups (MOH), and O in adsorbed H_2O, respectively [143]. But after adsorption of As(III) and As(V), the ratio of $O_{M\text{-}OH}$ to $O_{M\text{-}O}$ was changed from 0.96 to 0.87 and 0.88 respectively, which confirmed that Fe-OH groups were responsible for As(III) and As(V) adsorption by forming Fe–O-As bond through inner complex ligand exchange mechanism. The As(V) adsorption mechanism was explained on the surface of the AMP@Fe_2O_3 nanocomposite. Here, they found a point of zero charges of adsorbent before and after adsorption were 6.5 and 5.8 respectively. This shift in charge after adsorption was due to electrostatic attraction. Same time the FTIR bend of AMP@Fe_2O_3 nanocomposite for Fe–OH (1083 cm^{-1}) was removed and a new bend was seen at 807 cm^{-1} which also suggested that –OH groups were replaced by ligand exchange mechanism [144]. Zhou et al. also suggested oxygen-containing functional groups were responsible for As(V) on magnetic gelatin-modified biochar surfaces based on FTIR and XPS analysis. Singh et al. proposed the As(III) mechanism by monodentate corner-sharing 2C or 1 V complex formation and conversion to a bidentate edge-sharing 2C or 1 V complex [96].

In other studies, researchers found that As(III) was oxidized to As(V) by nano-zerovalent iron oxide nanoparticles, and then As(V) was attached to the adsorbent surface through electrostatic attraction [145–147]. Chitosan fibre-supported zero-valent iron nanoparticles were found the same types of results for As(III) and As(V) adsorption [148]. After the adsorption of As(III), the oxidation of Fe(0) was marked as the binding energy at 707 eV was shifting to higher energy bends which will be more favourable for As(V) adsorption. Again, the binding energy at 533.1 eV was for the more distinguished features for O in the As(V). This suggested that As(III) was largely oxidized to As(V) by nZVIO on the adsorbent surface (Fig. 7). The As(V) took place through electrostatic adsorption between protonated hydroxyl groups on the chitosan surface and $H_2AsO_4^{-}$/$HAsO_4^{2-}$ of As(V) species, respectively. Gupta et al. also found similar types of observation of As(III) adsorption through oxidation/adsorption on chitosan zerovalent iron nanoparticle surface [110].

Arsenic also adsorbs on the adsorbent surface by an ion exchange mechanism [149]. Majhi et al. found an ion-exchange mechanism for the adsorption of As(III) on the iron-oxide-coated natural rock surface [131, 132]. They found cation exchange was going on between Fe oxyhydroxides (=FeOOH) and As(III)-contained synthetic water, respectively. They found that first As(III) was converted to As(V) by the adsorbent and then As(V) was attached to iron-oxide-coated surfaces through –OH by weak hydrogen bonding and lastly attached on the adsorbent surface by elimination water.

4 Scope for Further Research

Based on the present review following future perspectives and challenges can be noted:

1. More agricultural by-products that are widely spread and go to waste without any use should be taken for activated carbon or biochar preparation, and then suitable iron oxide nanoparticles will be decorated to further increase the adsorption capacity for arsenic and other heavy metals.
2. Some biowaste and mining waste are combined with other materials, so without separating those creating a new bio-adsorbent will be helpful for arsenic removal studies.
3. The applicably of the adsorbent should not be for a single metalloid in the water. It should be applied for simultaneous decontamination of the groups of toxic pollutants such as Pb(II), Cd(II), Cr(VI), F^{-}, PO_4^{3-}, and toxic dyes.
4. Simulation studies should be done in pollutant removal studies which will increase the adsorption capacity, make easy the system, and be applied in real exercise.
5. Many studies are in lab-scale batch experiments, so it is very necessary to extend them to a specific contaminated area and calculate their potential at the industrial level.

5 Conclusion

The present review describes the use of iron oxide nanoparticles and a composite of iron oxide for arsenic removal in synthetic/natural water. The uses of chitosan, cellulose, activated carbon, biochar, and mining waste are biodegradable, low cost, environmentally friendly, easily available, and green in nature which acts as supporting material for iron oxide nanoparticles. The details of these composite properties and arsenic removal have been presented stepwise. The surface area, particle size, morphology, magnetic properties, and functional groups of the iron oxide-based adsorbent have been analyzed overly. On the other hand, the adsorption capacity, removal rate, and optimum conditions for arsenic removal are given in this study. The adsorption mechanism of arsenic has been point wise analyzed on the adsorbent surface. Overlay, the inner surface complex mechanism including monodentate and bidentate ligand exchange mechanism, and electrostatic attraction are responsible for the arsenic adsorption. The iron oxide with activated carbon,

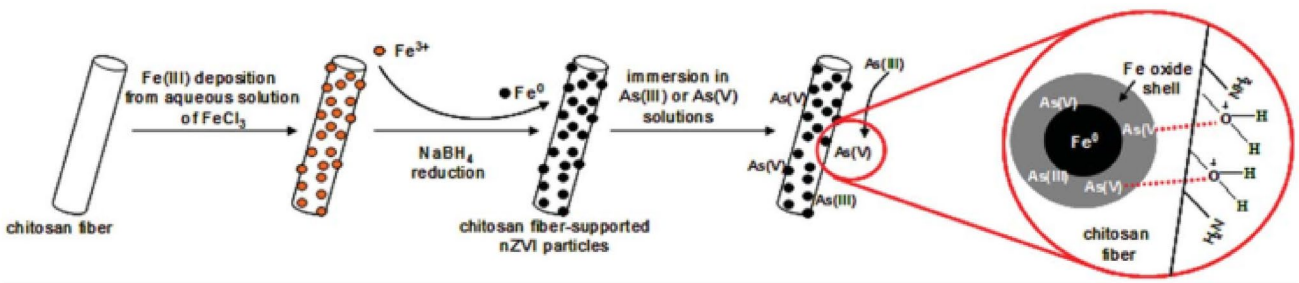

Fig. 7 Experimental steps for the preparation of chitosan fiber-supported nZVI particles and proposed mechanism of As(III)/As(V) sorption [148]

biochar, cellulose, and chitosan shows very good results for arsenic removal. Hence, they can play a crucial role in a bright future for arsenic removal in real wastewater and are highly helpful for rural area people across the world.

Acknowledgements The authors are thankful to the Chengdu University of Technology for providing all the necessary facilities.

Funding The authors declare that no funds, grants, or other support were received during the preparation of this manuscript.

Data availability Data is available on request.

Declarations

Conflict of Interest The authors declare no conflict of interest.

References

1. Xu J, Cao Z, Zhang Y, Yuan Z, Lou Z, Xu X et al (2018) A review of functionalized carbon nanotubes and graphene for heavy metal adsorption from water: preparation, application, and mechanism. Chemosphere 195:351–364
2. Ahmed FE, Lalia BS, Hashaikeh R (2015) A review on electrospinning for membrane fabrication: challenges and applications. Desalination 356:15–30
3. Bai B, Mi X, Xiang X, Heiden PA, Heldt CL (2013) Non-enveloped virus reduction with quaternized chitosan nanofibers containing graphene. Carbohydr Res 380:137–142
4. Carolin CF, Kumar PS, Saravanan A, Joshiba GJ, Naushad M (2017) Efficient techniques for the removal of toxic heavy metals from aquatic environment: a review. J Environ Chem Eng 5:2782–2799
5. Zazycki MA, Tanabe EH, Bertuol DA, Dotto GL (2017) Adsorption of valuable metals from leachates of mobile phone wastes using biopolymers and activated carbon. J Environ Manag 188:18–25
6. Savage N, Diallo MS (2005) Nanomaterials and water purification: opportunities and challenges. J Nanoparticle Res 7:331–342
7. Álvarez-Torrellas S, Peres JA, Gil-Álvarez V, Ovejero G, García J (2017) Effective adsorption of non-biodegradable pharmaceuticals from hospital wastewater with different carbon materials. Chem Eng J 320:319–329
8. Kalhor MM, Rafati AA, Rafati L, Rafati AA (2018) Synthesis, characterization and adsorption studies of amino functionalized silica nano hollow sphere as an efficient adsorbent for removal of imidacloprid pesticide. J Mol Liq 266:453–459
9. Sahu UK, Sahu MK, Mohapatra SS, Patel RK (2016) Removal of As(V) from aqueous solution by Ce-Fe bimetal mixed oxide. J Environ Chem Eng 4:2892–2899
10. Sahu MK, Sahu UK, Patel RK (2015) Adsorption of safranin-O dye on CO_2 neutralized activated red mud waste: process modelling, analysis and optimization using statistical design. RSC Adv 5:42294–42304
11. Sahu UK, Mahapatra SS, Patel RK (2018) Application of Box-Behnken Design in response surface methodology for adsorptive removal of arsenic from aqueous solution using CeO_2/Fe_2O_3/graphene nanocomposite. Mater Chem Phys 207:233–242
12. Ekka B, Nayak SR, Sathish KL, Achary S, Kumar A, Mawatwal S et al (2018) Synthesis of hydroxyapatite-zirconia nanocomposite through sonochemical route: a potential catalyst for degradation of phenolic compounds. J Environ Chem Eng 6:6504–6515
13. Ndimele PE, Kumolu-Joh CA, Chukwuka KS, Ndimele CC, Ayorinde OA, Adaramoye OR (2014) Phytoremediation of iron (Fe) and copper (Cu) by water hyacinth (*Eichhornia crassipes* (Mart.) Solms). Trends Appl Sci Res 2014:485–493
14. Peng K, Li X, Luo C, Shen Z (2006) Vegetation composition and heavy metal uptake by wild plants at three contaminated sites in Xiangxi area, China. J Environ Sci Heal Part A 41:65–76
15. Bhateria R, Singh R (2019) A review on nanotechnological application of magnetic iron oxides for heavy metal removal. J Water Process Eng 31:100845
16. Sahu MK, Mandal S, Dash SS, Badhai P, Patel RK (2013) Removal of Pb(II) from aqueous solution by acid activated red mud. J Environ Chem Eng 1:1315–1324
17. Sahu MK, Mandal S, Yadav LS, Dash SS, Patel RK (2016) Equilibrium and kinetic studies of Cd(II) ion adsorption from aqueous solution by activated red mud. Desalin Water Treat 57:14251–14265
18. AlOmar MK, Alsaadi MA, Jassam TM, Akib S, Ali HM (2017) Novel deep eutectic solvent-functionalized carbon nanotubes adsorbent for mercury removal from water. J Colloid Interface Sci 497:413–421
19. Sahu S, Sahu UK, Patel RK (2018) Synthesis of thorium-ethanolamine nanocomposite by the co-precipitation method and its application for Cr(VI) removal. New J Chem 42:5556–5569
20. Torasso N, Vergara-Rubio A, Pereira R, Martinez-Sabando J, Baudrit JRV, Cerveny S et al (2023) An in situ approach to entrap ultra-small iron oxide nanoparticles inside hydrophilic electrospun nanofibers with high arsenic adsorption. Chem Eng J 454:140168
21. Baig SA, Sheng T, Hu Y, Xu J, Xu X (2015) Arsenic removal from natural water using low cost granulated adsorbents: a review. Clean - Soil, Air, Water 43:13–26
22. Bissen M, Frimmel FH, Ag C (2003) Arsenic–a review. Part I : occurrence, toxicity, speciation mobility. Acta Hydrochim Hydrobiol 31:9–18
23. Hering JG, Katsoyiannis IA, Theoduloz GA, Berg M, Hug SJ (2017) Arsenic removal from drinking water: experiences with technologies and constraints in practice. J Environ Eng 143:1–9
24. Mohan D, Pittman CU (2007) Arsenic removal from water/wastewater using adsorbents: a critical review. J Hazard Mater 142:1–53
25. Hoque MA, Burgess WG, Ahmed KM (2017) Integration of aquifer geology, groundwater flow and arsenic distribution in deltaic aquifers: a unifying concept. Hydrol Process 31:2095–2109
26. Islam MS, Maamoun I, Falyouna O, Eljamal O, Saha BB (2023) Arsenic removal from contaminated water utilizing novel green composite *Chlorella vulgaris* and nano zero-valent iron. J Mol Liq 370:121005
27. Siddiqui SI, Chaudhry SA (2017) Iron oxide and its modified forms as an adsorbent for arsenic removal: a comprehensive recent advancement. Process Saf Environ Prot 111:592–626
28. Shan C, Tong M (2013) Efficient removal of trace arsenite through oxidation and adsorption by magnetic nanoparticles modified with Fe–Mn binary oxide. Water Res 47:3411–3421
29. Sahu UK, Sahu S, Mahapatra SS, Patel RK (2017) Cigarette soot activated carbon modified with Fe_3O_4 nanoparticles as an effective adsorbent for As(III) and As(V): material preparation, characterization and adsorption mechanism study. J Mol Liq 243:395–405
30. Hao L, Liu M, Wang N, Li G (2018) A critical review on arsenic removal from water using iron-based adsorbents. RSC Adv 8:39545–39560
31. Mudhoo A, Sharma SK, Garg VK, Tseng CH (2011) Arsenic: an overview of applications, health, and environmental concerns and removal processes. Crit Rev Environ Sci Technol 41:435–519

32. Tseng CH (2004) The potential biological mechanisms of arsenic-induced diabetes mellitus. Toxicol Appl Pharmacol 197:67–83
33. Wang YC, Chaung RH, Tung LC (2004) Comparison of the cytotoxicity induced by different exposure to sodium arsenite in two fish cell lines. Aquat Toxicol 69:67–79
34. Akter KF, Owens G, Davey DE, Naidu R (2006) Arsenic speciation and toxicity in biological systems. Rev Environ Contam Toxicol 184:97–149
35. Reid MS, Hoy KS, Schofield JRM, Uppal JS, Lin Y, Lu X et al (2020) Arsenic speciation analysis: a review with an emphasis on chromatographic separations. Trends Anal Chem 123:115770
36. Ochedi FO, Liu Y, Hussain A (2020) A review on coal fly ash-based adsorbents for mercury and arsenic removal. J Clean Prod 267:122143
37. Farnfield HR, Marcilla AL, Ward NI (2012) Arsenic speciation and trace element analysis of the volcanic río Agrio and the geothermal waters of Copahue, Argentina. Sci Total Environ 433:371–378
38. Guo Q, He T, Wu Q, Liu M (2020) Constraints of major ions and arsenic on the geological genesis of geothermal water: insight from a comparison between Xiong'an and Yangbajain, two hydrothermal systems in China. Appl Geochem 117:104589
39. Hoffmann N, Tortella G, Hermosilla E, Fincheira P, Diez MC, Lourenço IM et al (2022) Comparative toxicity assessment of eco-friendly synthesized superparamagnetic iron oxide nanoparticles (SPIONs) in plants and aquatic model organisms. Minerals 12:451
40. Chung JY, Do YuS, Hong YS (2014) Environmental source of arsenic exposure. J Prev Med Public Heal 47:253–257
41. Yang H, Han M, Jiang P (2021) Research Progress on the treatment of arsenic pollution by manganese oxide. E3S Web Conf 261:04032
42. Yadav MK, Saidulu D, Gupta AK, Ghosal PS, Mukherjee A (2021) Status and management of arsenic pollution in groundwater: a comprehensive appraisal of recent global scenario, human health impacts, sustainable field-scale treatment technologies. J Environ Chem Eng 9:105203
43. Aiuppa A, D'Alessandro W, Federico C, Palumbo B, Valenza M (2003) The aquatic geochemistry of arsenic in volcanic groundwaters from southern Italy. Appl Geochem 18:1283–1296
44. Liu R, Qu J (2021) Review on heterogeneous oxidation and adsorption for arsenic removal from drinking water. J Environ Sci 110:178–188
45. Basu A, Saha D, Saha R, Ghosh T, Saha B (2014) A review on sources, toxicity and remediation technologies for removing arsenic from drinking water. Res Chem Intermed 40:447–485
46. Asadi Haris S, Dabagh S, Mollasalehi H, Ertas YN (2023) Alginate coated superparamagnetic iron oxide nanoparticles as nanocomposite adsorbents for arsenic removal from aqueous solutions. Sep Purif Technol 310:123193
47. Cutter GA (1992) Kinetic controls on metalloid speciation in seawater. Mar Chem 40:65–80
48. Andjelkovic I, Azari S, Erkelens M, Forward P, Lambert MF, Losic D (2017) Bacterial iron-oxide nanowires from biofilm waste as a new adsorbent for the removal of arsenic from water. RSC Adv 7:3941–3948
49. John Y, David VE, Mmereki D (2018) A comparative study on removal of hazardous anions from water by adsorption: a review. Int J Chem Eng 2018:1–21
50. Ahmad P, Alam P, Balawi TH, Altalayan FH, Ahanger A, Ashraf M (2020) Sodium nitroprusside (SNP) improves tolerance to arsenic (As) toxicity in *Vicia faba* through the modifications of biochemical attributes, antioxidants, ascorbate- glutathione cycle and glyoxalase cycle. Chemosphere 244:125480
51. Bali AS, Sidhu GPS (2021) Arsenic acquisition, toxicity and tolerance in plants - from physiology to remediation: a review. Chemosphere 283:131050
52. Ventura-Lima J, Bogo MR, Monserrat JM (2011) Arsenic toxicity in mammals and aquatic animals: a comparative biochemical approach. Ecotoxicol Environ Saf 74:211–218
53. Sarkar A, Paul B (2016) The global menace of arsenic and its conventional remediation: a critical review. Chemosphere 158:37–49
54. Bahmani P, Maleki A, Daraei H, Khamforoush M, Rezaee R, Gharibi F et al (2017) High-flux ultrafiltration membrane based on electrospun polyacrylonitrile nanofibrous scaffolds for arsenate removal from aqueous solutions. J Colloid Interface Sci 506:564–571
55. Bolisetty S, Peydayesh M, Mezzenga R (2019) Sustainable technologies for water purification from heavy metals: review and analysis. Chem Soc Rev 48:463–487
56. Zakhar R, Derco J, Čacho F (2018) An overview of main arsenic removal technologies. Acta Chim Slovaca 11:107–113
57. Sun T, Zhao Z, Liang Z, Liu J, Shi W, Cui F (2017) Efficient As(III) removal by magnetic CuO-Fe_3O_4 nanoparticles through photo-oxidation and adsorption under light irradiation. J Colloid Interface Sci 495:168–177
58. Ortega A, Oliva I, Contreras KE, Rivero EP, Technology P, Oliva I et al (2017) Arsenic removal from water by hybrid electroregenerated anion exchange resin/electrodialysis process. Sep Purif Technol 184:319–326
59. Chowdhury R (2017) Using adsorption and sulphide precipitation as the principal removal mechanisms of arsenic from a constructed wetland–a critical review. Chem Ecol 33:560–571
60. Hayati B, Maleki A, Najafi F, Daraei H, Gharibi F, McKay G (2017) Adsorption of Pb^{2+}, Ni^{2+}, Cu^{2+}, Co^{2+} metal ions from aqueous solution by PPI/SiO_2 as new high performance adsorbent: preparation, characterization, isotherm, kinetic, thermodynamic studies. J Mol Liq 237:428–436
61. Hua M, Zhang S, Pan B, Zhang W, Lv L, Zhang Q (2012) Heavy metal removal from water/wastewater by nanosized metal oxides: a review. J Hazard Mater 211–212:317–331
62. Ghosh S, Prabhakar R, Samadder SR (2019) Performance of γ-aluminium oxide nanoparticles for arsenic removal from groundwater. Clean Technol Environ Policy 21:121–138
63. Li R, Li Q, Gao S, Shang JK (2012) Exceptional arsenic adsorption performance of hydrous cerium oxide nanoparticles: part A. Adsorption capacity and mechanism. Chem Eng J 185–186:127–135
64. Li W, Chen D, Xia F, Tan JZY, Huang PP, Song WG et al (2016) Extremely high arsenic removal capacity for mesoporous aluminium magnesium oxide composites. Environ Sci Nano 3:94–106
65. Hou J, Luo J, Song S, Li Y, Li Q (2016) The remarkable effect of the coexisting arsenite and arsenate species ratios on arsenic removal by manganese oxide. Chem Eng J 315:159–166
66. Guan X, Du J, Meng X, Sun Y, Sun B, Hu Q (2012) Application of titanium dioxide in arsenic removal from water: a review. J Hazard Mater 215–216:1–16
67. Li Y, Liu Z, Li Q, Zhao Z, Liu Z, Zeng L et al (2011) Removal of arsenic from arsenate complex contained in secondary zinc oxide. Hydrometallurgy 109:237–244
68. Scott KN, Green JF, Do HD, McLean SJ (1995) Arsenic removal by coagulation with aluminium, iron, titanium, and zirconium. J Am Water Works Assoc 87:114–126
69. Nekhunguni PM, Tavengwa NT, Tutu H (2017) Investigation of As(V) removal from acid mine drainage by iron (hydr) oxide modified zeolite. J Environ Manage 197:550–558
70. Zhang X, Fang X, Li J, Pan S, Sun X, Han W et al (2018) Developing new adsorptive membrane by modification of support layer

with iron oxide microspheres for arsenic removal. J Colloid Interface Sci 514:760–768
71. Tuna AÖA, Özdemir E, Şimşek EB, Beker U (2013) Removal of As(V) from aqueous solution by activated carbon-based hybrid adsorbents: impact of experimental conditions. Chem Eng J 223:116–128
72. Su H, Ye Z, Hmidi N (2017) High-performance iron oxide – graphene oxide nanocomposite adsorbents for arsenic removal. Colloids Surfaces A Physicochem Eng Asp 522:161–172
73. Kumar P, Tomar V, Kumar D, Joshi RK, Nemiwal M (2022) Magnetically active iron oxide nanoparticles for catalysis of organic transformations: a review. Tetrahedron 106–107:132641
74. Raul PK, Devi RR, Umlong IM, Thakur AJ, Banerjee S, Veer V (2014) Iron oxide hydroxide nanoflower assisted removal of arsenic from water. Mater Res Bull 49:360–368
75. Song K, Kim W, Suh CY, Shin D, Ko KS, Ha K (2013) Magnetic iron oxide nanoparticles prepared by electrical wire explosion for arsenic removal. Powder Technol 246:572–574
76. Mayo JT, Yavuz C, Yean S, Cong L, Shipley H, Yu W et al (2007) The effect of nanocrystalline magnetite size on arsenic removal. Sci Technol Adv Mater 8:71–75
77. Chowdhury SR, Yanful EK (2011) Arsenic removal from aqueous solutions by adsorption on magnetite nanoparticles. Water Environ J 25:429–437
78. Chowdhury SR, Yanful EK, Pratt AR (2011) Arsenic removal from aqueous solutions by mixed magnetite-maghemite nanoparticles. Environ Earth Sci 64:411–423
79. Luther S, Borgfeld N, Kim J, Parsons JG (2012) Removal of arsenic from aqueous solution: a study of the effects of pH and interfering ions using iron oxide nanomaterials. Microchem J 101:30–36
80. Sahu UK, Sahu MK, Mahapatra SS, Patel RK (2017) Removal of As(III) from Aqueous solution using Fe_3O_4 nanoparticles : process modeling and optimization using statistical design. Water Air Soil Pollut 228:1–15
81. Kilianová M, Prucek R, Filip J, Kolařík J, Kvítek L, Panáček A et al (2013) Remarkable efficiency of ultrafine superparamagnetic iron(III) oxide nanoparticles toward arsenate removal from aqueous environment. Chemosphere 93:2690–2697
82. Cheng W, Xu J, Wang Y, Wu F, Xu X, Li J (2015) Dispersion-precipitation synthesis of nanosized magnetic iron oxide for efficient removal of arsenite in water. J Colloid Interface Sci 445:93–101
83. Das GK, Bonifacio CS, De Rojas J, Liu K, Van Benthem K, Kennedy IM (2014) Ultra-long magnetic nanochains for highly efficient arsenic removal from water. J Mater Chem A 2:12974–12981
84. Vicente-Martínez Y, Caravaca M, El FS, Hernández-Córdoba M, López-García I (2023) Magnetic nanoparticles for removing inorganic arsenic species from waters: a proof of concept for potential application. Adv Sample Prep 6:100064
85. Pabón Reyes DC, Halac EB, Litter MI (2023) As(III) removal of aqueous solutions using zerovalent iron nanoparticles: the role of the UVA-Vis irradiation wavelength. J Photochem Photobiol A Chem 443:114846
86. Piraján JCM, Giraldo L (2013) Activated carbon from bamboo waste modified with iron and its application in the study of the adsorption of arsenite and arsenate. Cent Eur J Chem 11:160–170
87. Liu Z, Zhang FS, Sasai R (2010) Arsenate removal from water using Fe_3O_4-loaded activated carbon prepared from waste biomass. Chem Eng J 160:57–62
88. Maiti A, Agarwal V, De S, Basu JK (2010) Removal of As(V) using iron oxide impregnated carbon prepared from Tamarind hull. J Environ Sci Heal - Part A 45:1207–1216
89. Yürüm A, Kocabaş-Atakli ZÖ, Sezen M, Semiat R, Yürüm Y (2014) Fast deposition of porous iron oxide on activated carbon by microwave heating and arsenic (V) removal from water. Chem Eng J 242:321–332
90. Kalaruban M, Loganathan P, Nguyen TV, Nur T, Hasan Johir MA, Nguyen TH et al (2019) Iron-impregnated granular activated carbon for arsenic removal: application to practical column filters. J Environ Manag 239:235–243
91. Zhu H, Jia Y, Wu X, Wang H (2009) Removal of arsenic from water by supported nano zero-valent iron on activated carbon. J Hazard Mater 172:1591–1596
92. Zhang F, Wang X, Xionghui J, Ma L (2016) Efficient arsenate removal by magnetite-modified water hyacinth biochar. Environ Pollut 216:575–583
93. Wei Y, Wei S, Liu C, Chen T, Tang Y, Ma J et al (2019) Efficient removal of arsenic from groundwater using iron oxide nanoneedle array-decorated biochar fibers with high Fe utilization and fast adsorption kinetics. Water Res 167:115107
94. Liu X, Ao H, Xiong X, Xiao J, Liu J (2012) Arsenic removal from water by iron-modified bamboo charcoal. Water Air Soil Pollut 223:1033–1044
95. Zhou Z, Liu YG, Liu SB, Liu HY, Zeng GM, Tan XF et al (2017) Sorption performance and mechanisms of arsenic(V) removal by magnetic gelatin-modified biochar. Chem Eng J 314:223–231
96. Singh P, Sarswat A, Pittman CU, Mlsna T, Mohan D (2020) Sustainable low-concentration arsenite [As(III)] removal in single and multicomponent systems using hybrid iron oxide-biochar nanocomposite adsorbents: a mechanistic study. ACS Omega 5:2575–2593
97. Duan X, Zhang C, Srinivasakannan C, Wang X (2017) Waste walnut shell valorization to iron loaded biochar and its application to arsenic removal. Resour Technol 3:29–36
98. Dhoble RM, Maddigapu PR, Bhole AG, Rayalu S (2018) Development of bark-based magnetic iron oxide particle (BMIOP), a bio-adsorbent for removal of arsenic (III) from water. Environ Sci Pollut Res 25:19657–19674
99. Sahu UK, Sahu S, Mahapatra SS, Patel RK (2019) Synthesis and characterization of magnetic bio-adsorbent developed from *Aegle marmelos* leaves for removal of As(V) from aqueous solutions. Environ Sci Pollut Res 26:946–958
100. Olivera S, Muralidhara HB, Venkatesh K, Guna VK, Gopalakrishna K, Kumar KY (2016) Potential applications of cellulose and chitosan nanoparticles/composites in wastewater treatment: a review. Carbohydr Polym 153:600–618
101. Kanematsu M, Young TM, Fukushi K, Green PG, Darby JL (2013) Arsenic(III, V) adsorption on a goethite-based adsorbent in the presence of major co-existing ions: modeling competitive adsorption consistent with spectroscopic and molecular evidence. Geochim Cosmochim Acta 106:404–428
102. He J, Bardelli F, Gehin A, Silvester E, Charlet L (2016) Novel chitosan goethite bionanocomposite beads for arsenic remediation. Water Res 101:1–9
103. Liu C, Wang B, Deng Y, Cui B, Wang J, Chen W et al (2015) Performance of a new magnetic chitosan nanoparticle to remove arsenic and its separation from water. J Nanomater 191829:1–9
104. Abdollahi M, Zeinali S, Nasirimoghaddam S, Sabbaghi S (2015) Effective removal of As (III) from drinking water samples by chitosan-coated magnetic nanoparticles. Desalin Water Treat 56:2092–2104
105. Chauhan D, Dwivedi J, Sankararamakrishnan N (2014) Novel chitosan/PVA/zerovalent iron biopolymeric nanofibers with enhanced arsenic removal applications. Environ Sci Pollut Res 21:9430–9442
106. Zeng J, Qi P, Shi J, Pichler T, Wang F, Wang Y et al (2020) Chitosan functionalized iron nanosheet for enhanced removal of As(III) and Sb(III): synergistic effect and mechanism. Chem Eng J 382:122999

107. Liu S, Huang B, Chai L, Liu Y, Zeng G, Wang X et al (2017) Enhancement of As(v) adsorption from aqueous solution by a magnetic chitosan/biochar composite. RSC Adv 7:10891–10900
108. Gupta A, Yunus M, Sankararamakrishnan N (2013) Chitosan- and iron-chitosan-coated sand filters: a cost-effective approach for enhanced arsenic removal. Ind Eng Chem Res 52:2066–2072
109. Gupta A, Chauhan VS, Sankararamakrishnan N (2009) Preparation and evaluation of iron-chitosan composites for removal of As(III) and As(V) from arsenic contaminated real life groundwater. Water Res 43:3862–3870
110. Gupta A, Yunus M, Sankararamakrishnan N (2012) Zerovalent iron encapsulated chitosan nanospheres - a novel adsorbent for the removal of total inorganic Arsenic from aqueous systems. Chemosphere 86:150–155
111. Hokkanen S, Repo E, Sillanpää M (2013) Removal of heavy metals from aqueous solutions by succinic anhydride modified mercerized nanocellulose. Chem Eng J 223:40–47
112. Habibi Y, Lucia LA, Rojas OJ (2010) Cellulose nanocrystals: chemistry, self-assembly, and applications. Chem Rev 110:3479–3500
113. Setyono D, Valiyaveettil S (2014) Chemically modified sawdust as renewable adsorbent for arsenic removal from water. ACS Sustain Chem Eng 2:2722–2729
114. Mamindy-Pajany Y, Hurel C, Marmier N, Roméo M (2011) Arsenic (V) adsorption from aqueous solution onto goethite, hematite, magnetite and zero-valent iron: effects of pH, concentration and reversibility. Desalination 281:93–99
115. Du Z, Zheng T, Wang P, Hao L, Wang Y (2016) Fast microwave-assisted preparation of a low-cost and recyclable carboxyl modified lignocellulose-biomass jute fiber for enhanced heavy metal removal from water. Bioresour Technol 201:41–49
116. Tuutijärvi T, Lu J, Sillanpää M, Chen G (2009) As(V) adsorption on maghemite nanoparticles. J Hazard Mater 166:1415–1420
117. Liu S, Zhang L, Zhou J, Wu R (2008) Structure and properties of cellulose/Fe_2O_3 nanocomposite fibers spun via an effective pathway. J Phys Chem C 112:4538–4544
118. Yu X, Tong S, Ge M, Zuo J, Cao C, Song W (2013) One-step synthesis of magnetic composites of cellulose@iron oxide nanoparticles for arsenic removal. J Mater Chem A 1:959–965
119. Zhou S, Wang D, Sun H, Chen J, Wu S, Na P (2014) Synthesis, characterization, and adsorptive properties of magnetic cellulose nanocomposites for arsenic removal. Water Air Soil Pollut 225:1–13
120. Hokkanen S, Repo E, Lou S, Sillanpää M (2015) Removal of arsenic(V) by magnetic nanoparticle activated microfibrillated cellulose. Chem Eng J 260:886–894
121. Tian Y, Wu M, Lin X, Huang P, Huang Y (2011) Synthesis of magnetic wheat straw for arsenic adsorption. J Hazard Mater 193:10–16
122. Hao L, Zheng T, Jiang J, Hu Q, Li X, Wang P (2015) Removal of As(iii)from water using modified jute fibres as a hybrid adsorbent. RSC Adv 5:10723–10732
123. Sahu UK, Mahapatra SS, Patel RK (2017) Synthesis and characterization of an eco-friendly composite of jutefiber and Fe_2O_3 nanoparticles and its application as an adsorbent for removal of As(V) from water. J Mol Liq 237:313–321
124. Lunge S, Singh S, Sinha A (2014) Magnetic iron oxide (Fe_3O_4) nanoparticles from tea waste for arsenic removal. J Magn Magn Mater 356:21–31
125. Sheng T, Baig SA, Hu Y, Xue X, Xu X (2014) Development, characterization and evaluation of iron-coated honeycomb briquette cinders for the removal of As(V) from aqueous solutions. Arab J Chem 7:27–36
126. Ren G, Wang X, Zheng B, Zhang Z, Yang L, Yang X (2020) Fabrication of Mg doped magnetite nanoparticles by recycling of titanium slag and their application of arsenate adsorption. J Clean Prod 252:119599
127. Yigit E, Yurtsever A, Basaran ST, Sahinkaya E (2020) Optimization of arsenic removal from an acid mine drainage in an anaerobic membrane bioreactor. Environ Technol Innov 18:100712
128. Mahmodi G, Zarrintaj P, Taghizadeh A, Taghizadeh M, Manouchehri S, Dangwal S et al (2020) From microporous to mesoporous mineral frameworks: an alliance between zeolite and chitosan. Carbohydr Res 489:107930
129. Sithole NT, Ntuli F, Okonta F (2020) Fixed bed column studies for decontamination of acidic mineral effluent using porous fly ash-basic oxygen furnace slag based geopolymers. Miner Eng 154:106397
130. Devi RR, Umlong IM, Das B, Borah K, Thakur AJ, Raul PK et al (2014) Removal of iron and arsenic (III) from drinking water using iron oxide-coated sand and limestone. Appl Water Sci 4:175–182
131. Maji SK, Kao YH, Liu CW (2011) Arsenic removal from real arsenic-bearing groundwater by adsorption on iron-oxide-coated natural rock (IOCNR). Desalination 280:72–79
132. Maji SK, Kao YH, Wang CJ, Lu GS, Wu JJ, Liu CW (2012) Fixed bed adsorption of As(III) on iron-oxide-coated natural rock (IOCNR) and application to real arsenic-bearing groundwater. Chem Eng J 203:285–293
133. Srivastava D, Vaishya RC (2015) Treatment of arsenic (III) contaminated water by dynamically modified iron-coated sand (DMICS). Desalin Water Treat 53:2565–2577
134. Haque N, Morrison G, Cano-Aguilera I, Gardea-Torresdey JL (2008) Iron-modified light expanded clay aggregates for the removal of arsenic(V) from groundwater. Microchem J 88:7–13
135. Pawar RR, Lalhmunsiama KM, Kim JG, Hong SM, Sawant SY et al (2018) Efficient removal of hazardous lead, cadmium, and arsenic from aqueous environment by iron oxide modified clay-activated carbon composite beads. Appl Clay Sci 162:339–350
136. Tandon PK, Shukla RC, Singh SB (2013) Removal of arsenic(III) from water with clay-supported zerovalent iron nanoparticles synthesized with the help of tea liquor. Ind Eng Chem Res 52:10052–10058
137. Liu CH, Chuang YH, Chen TY, Tian Y, Li H, Wang MK et al (2015) Mechanism of arsenic adsorption on magnetite nanoparticles from water: thermodynamic and spectroscopic studies. Environ Sci Technol 49:7726–7734
138. Liang Y, Min X, Chai L, Wang M, Liyang W, Pan Q et al (2017) Stabilization of arsenic sludge with mechanochemically modified zero valent iron. Chemosphere 168:1142–1151
139. Thi TM, Trang NTH, Van Anh NT (2015) Effects of Mn, Cu doping concentration to the properties of magnetic nanoparticles and arsenic adsorption capacity in wastewater. Appl Surf Sci 340:166–172
140. Tofan-Lazar J, Al-Abadleh HA (2012) Kinetic ATR-FTIR studies on phosphate adsorption on iron (Oxyhydr)oxides in the absence and presence of surface arsenic: molecular-level insights into the Ligand exchange mechanism. J Phys Chem A 116:10143–10149
141. Morin G, Ona-Nguema G, Wang Y, Menguy N, Juillot F, Proux O et al (2008) Extended X-ray absorption fine structure analysis of arsenite and arsenate adsorption on maghemite. Environ Sci Technol 42:2361–2366
142. Buschmann J, Kappeler A, Lindauer U, Kistler D, Berg M, Sigg L (2006) Arsenite and arsenate binding to dissolved humic acids: influence of pH, type of humic acid, and aluminum. Environ Sci Technol 40:6015–6020
143. Liu J, Ge X, Ye X, Wang G, Zhang H, Zhou H et al (2016) 3D graphene/δ-MnO_2 aerogels for highly efficient and reversible removal of heavy metal ions. J Mater Chem A 4:1970–1979

144. Tian N, Tian X, Ma L, Yang C, Wang Y, Wang Z et al (2015) Well-dispersed magnetic iron oxide nanocrystals on sepiolite nanofibers for arsenic removal. RSC Adv 5:25236–25243
145. Kanel SR, Manning B, Charlet L, Choi H (2005) Removal of arsenic(III) from groundwater by nanoscale zero-valent iron. Environ Sci Technol 39:1291–1298
146. Ramos MAV, Weile Y, Li XQ, Koel BE, Zhang WX (2009) Simultaneous oxidation and reduction of arsenic by zero-valent iron nanoparticles: understanding the significance of the core-shell structure. J Phys Chem C 113:14591–14594
147. Yan W, Ramos MAV, Koel BE, Zhang WX (2010) Multi-tiered distributions of arsenic in iron nanoparticles: observation of dual redox functionality enabled by a core-shell structure. Chem Commun 46:6995–6997
148. Horzum N, Demir MM, Nairat M, Shahwan T (2013) Chitosan fiber-supported zero-valent iron nanoparticles as a novel sorbent for sequestration of inorganic arsenic. RSC Adv 3:7828–7837
149. Mills SJ, Christy AG, Génin J-MR, Kameda T, Colombo F (2012) Nomenclature of the hydrotalcite supergroup: natural layered double hydroxides. Mineral Mag 76:1289–1336